



Positive feedback of
dust aerosol

S. Remy et al.

This discussion paper is/has been under review for the journal Atmospheric Chemistry and Physics (ACP). Please refer to the corresponding final paper in ACP if available.

Positive feedback of dust aerosol via its impact on atmospheric stability during dust storms in the Eastern Mediterranean

S. Remy^{1,2}, A. Benedetti¹, T. Haiden¹, L. Jones¹, M. Razinger¹, J. Flemming¹, R. J. Engelen¹, V. H. Peuch¹, and J. N. Thepaut¹

¹European Centre for Medium-range Weather Forecasts, Reading, UK

²Laboratoire de Météorologie Dynamique, Paris, France

Received: 28 August 2014 – Accepted: 8 October 2014 – Published: 13 November 2014

Correspondence to: S. Remy (samuel.remy@ecmwf.int)

Published by Copernicus Publications on behalf of the European Geosciences Union.

Title Page

Abstract

Introduction

Conclusions

References

Tables

Figures



Back

Close

Full Screen / Esc

Printer-friendly Version

Interactive Discussion



Abstract

Aerosols affect the atmosphere through the aerosol-radiation and the aerosol-clouds interactions. In this paper we report on a new mechanism whereby the radiative effect of dust aerosol on surface fluxes acts to increase the dust loading of the atmosphere via modification of boundary-layer stability, thereby acting to enhance the radiative aerosol effect. This positive feedback between dust aerosol and boundary layer stability occurred during a series of dust storms in the Sahara and the Eastern Mediterranean in April 2012, which were studied using the Monitoring Atmospheric Composition and Climate – Interim Implementation (MACC-II) system.

The radiative fluxes in the shortwave and long-wave spectra were both significantly affected by the prognostic aerosols-radiation interaction, which strongly influenced the meteorological simulation. Reduced incoming solar radiation below the aerosol layers caused a decrease in maximum surface temperatures, and consequently a more stable thermal stratification of the lower atmosphere. The increased thermal stability led to decreased surface wind speeds and therefore to smaller amounts of dust aerosol emissions. Larger downwelling long-wave fluxes were associated with the opposite processes: less stable thermal stratification at night, brought mainly by higher minimum temperatures at the surface, caused stronger surface winds. Overall, the impact by the long-wave radiative forcing was more important than the short-wave contribution.

This feedback was amplified when taken into account in the aerosol analysis of the MACC-II global system. It led to a notable improvement in short term forecast of short and long-wave radiative fluxes, of surface temperature but also of the aerosol burden itself. Forecasts of radiative fluxes in the shortwave and long-wave spectrum were also improved. At a longer range the improvement were less important as the forecast error of the aerosol load increased, thereby highlighting the importance of accurate aerosol representation in the study of aerosol-radiation interaction.

Positive feedback of dust aerosol

S. Remy et al.

Title Page

Abstract

Introduction

Conclusions

References

Tables

Figures



Back

Close

Full Screen / Esc

Printer-friendly Version

Interactive Discussion



1 Introduction

1.1 Aerosol impacts on meteorology

Aerosol particles play an important role in the atmosphere through various mechanisms. They impact air quality and represent a serious public health issue, as shown by recent Particulate Matter (PM) pollution events in Western Europe and China (Zhang et al., 2014; Sun et al., 2013). Aerosol particles also influence the atmospheric radiative budget through the aerosol-radiation interaction, also called aerosol direct effect (Yu et al., 2006; Bellouin et al., 2005), by scattering and absorbing short-wave and long-wave radiation, and through the aerosol-clouds interaction or aerosol semi direct and indirect effect, by influencing the concentration, size and chemical composition of the cloud condensation nuclei (CCN), which in turn impacts the life cycle, the optical properties and the precipitation activity of clouds (Koch et al., 2010; Painemal et al., 2013).

The aerosol direct effect consists of the sum of two phenomena: scattering/absorption of incoming solar radiation and absorption/emission of long-wave radiation. The former reduces the amount of solar energy that reaches the surface and as a consequence lessens the intensity of day-time warming of the surface. Black carbon particles however, can cause a warming in the atmosphere because of absorption. Aerosols also absorb and reemit long-wave radiation, which increases down-welling surface long-wave radiation in and below the aerosol layer, and reduces night-time cooling of the surface. An aerosol layer thus acts on the radiative budget at the surface and in the lower atmosphere similar to a thin layer of clouds. The radiative impact of aerosols is very dependent on their vertical distribution: Choi and Chung (2014) showed that whether the aerosol layer is below or above a cloud layer will impact their radiative impact by an order of magnitude. Overall, on climatic time scales, the cooling impacts at the surface caused by the aerosol direct effect dominate the warming effect: the radiative contribution of aerosols at the surface is estimated by the Intergovernmental Panel on Climate Change (IPCC) to be in the range of -0.3 W m^{-2} (IPCC, 2013).

Positive feedback of dust aerosol

S. Remy et al.

Title Page

Abstract

Introduction

Conclusions

References

Tables

Figures



Back

Close

Full Screen / Esc

Printer-friendly Version

Interactive Discussion



Positive feedback of dust aerosol

S. Remy et al.

Title Page

Abstract

Introduction

Conclusions

References

Tables

Figures



Back

Close

Full Screen / Esc

Printer-friendly Version

Interactive Discussion



This is in line with the results of the AeroCom project (Schulz et al., 2006; Stier et al., 2013), with a mean radiative impact of aerosols evaluated at -0.22 W m^{-2} . In both cases, uncertainties on the radiative impacts of the aerosols are relatively high, associated with uncertainties on the quantification of aerosol sources and the interaction of aerosols with themselves and with the hydrological cycle (IPCC, 2013) interactions.

As aerosol particles impact the radiative budget at the surface and also the thermal stratification of the lower atmosphere through the direct effect, other atmospheric processes are affected as well, in the Planetary Boundary Layer (PBL) and above. Increased surface temperatures at night will decrease the stability of the lower atmosphere, thus enhancing turbulent diffusion. Lower maximum temperatures will on the other hand decrease turbulent diffusion of heat. Since temperature and wind patterns are linked, the presence of an aerosol layer will also have an impact on wind patterns. Different heat diffusion and wind patterns can influence meso-scale and synoptic weather systems: Reale et al. (2011) for example showed that the African Easterly Jet (AEJ) was forecasted at an altitude and position that was closer to observations with interactive aerosols radiative effect. Heinhold et al. (2008) also showed how the radiative effects of aerosols impacted the Low Level Jet (LLJ) in the Bodele depression of South Sahara, thus enhancing dust aerosol production. Dust aerosol events over the Eastern Atlantic may also impact hurricane activity over the Atlantic and Caribbean areas (Kamal et al., 2012 and S. H. Chen, personal communication, 2014).

Most climate models now include aerosols and take into account their radiative impact on the atmosphere (Bellouin et al., 2011). For operational Numerical Weather Prediction (NWP) models, Tompkins et al. (2005) showed that taking into account the aerosol radiative impacts through an aerosol climatology significantly improved the skill of the weather forecasts by the European Centre for Medium-Range Weather Forecasts (ECMWF) operational model. More recently, Rodwell and Jung (2008) used a monthly aerosol climatology instead of a fixed climatology with a positive impact on global circulation forecasts by the same model. Mulcahy et al. (2014) investigated several configurations for the inclusion of interactive aerosol direct and indirect effects in

the Met Office Unified Model (MetUM) and managed to correct a significant bias in the outgoing long-wave radiative fluxes over the Sahara that was diagnosed by Haywood et al. (2005).

This paper aims to document the interaction between the lower atmosphere and dust aerosols during a series of dust storm in the Sahara. In particular, the various feedbacks between the radiative impact of aerosols on the shortwave or long-wave spectra on one hand, and boundary layer meteorological processes on the other hand, were analyzed. The interaction of prognostic aerosols and meteorology were included at first only in the forward model, without any impact on the dust aerosol initial conditions. In a second step, they were included in the aerosol assimilation system so that the initial conditions of dust aerosols also took into account the impact of this interaction. Experiments using prognostic aerosols on one hand, and an aerosol climatology on the other hand for the computation of the aerosol-radiation interaction were compared. This allowed to assess the benefits of using prognostic aerosols instead of a climatology to estimate the aerosol impacts on meteorological fields.

1.2 The MACC global atmospheric composition forecasting system

The Monitoring Atmospheric Composition and Climate – Interim Implementation (MACC-II) is a European funded program that aims at monitoring and forecasting atmospheric composition. It is the precursor of the broader Copernicus Atmosphere Monitoring Service. MACC-II's aim is to create and operate an assimilation and forecasting system for monitoring aerosols, greenhouse gases and reactive gases, using satellite observations and a combination of global and regional models (Hollingsworth et al., 2008; Peuch and Engelen, 2012).

Aerosols are forecasted within the MACC-II global system by a forward model (Morcrette et al., 2009, based on earlier work by Reddy et al., 2005 and Boucher et al., 2002) that uses five species: dust, sea-salt, black carbon, organic carbon and sulfates. Dust aerosols are represented by three prognostic variables that correspond to three bins, with bin limits of 0.03, 0.55, 0.9 and 20 μm . The main processes that are taken

Positive feedback of dust aerosol

S. Remy et al.

Title Page

Abstract

Introduction

Conclusions

References

Tables

Figures



Back

Close

Full Screen / Esc

Printer-friendly Version

Interactive Discussion



Positive feedback of dust aerosol

S. Remy et al.

Title Page

Abstract

Introduction

Conclusions

References

Tables

Figures



Back

Close

Full Screen / Esc

Printer-friendly Version

Interactive Discussion



into account are production of dust aerosols through saltation and removal by dry deposition and sedimentation. The areas likely to produce dust aerosols are diagnosed as a function of surface albedo, moisture of the first soil level and bare soil fraction. Dust sources are then parameterized, following Ginoux (2001), as a function of the cubic power of 10 m wind speed. Dry deposition depends on a prescribed deposition velocity and on aerosol concentration in the lowermost model level above the surface. Sedimentation is currently applied only to the largest dust aerosol bin and depends on a fixed settling velocity and the concentration at each model level.

In the pre-operational version of the global MACC-II system, the radiative impact of aerosols is taken into account using the aerosol monthly climatology of Tegen et al. (1997). In an experimental version of the model, the aerosol direct effect can be computed from the prognostic aerosols provided by the MACC aerosol module. It is also possible to activate only the short-wave or the long-wave components of the aerosol direct effect separately.

The global MACC-II forecasting system provides aerosol analysis by assimilating total Aerosol Optical Depth (AOD) observations provided by the Moderate Resolution Imaging Spectroradiometer (MODIS) instruments on-board NASA's polar orbiting satellites Aqua and Terra in a 4D-Var assimilation algorithm, as described in Benedetti et al. (2009). The product used in the assimilation step is the Dark Target retrieval, hence not available in regions with high surface albedo, such as desert areas. The use of the MODIS Deep Blue product, aimed at bright surfaces, is currently under investigation.

1.3 Evaluating aerosol impacts on numerical weather prediction: WGNE model inter-comparison

The Working Group on Numerical Experimentation (WGNE) was jointly established by the Commission for Atmospheric Sciences of the World Meteorological Organization (WMO) and the World Climate Research Programme (WCRP). It has the responsibility of fostering the development of atmospheric circulation models for use in weather, climate, water and environmental prediction on all time scales and diagnosing and

resolving shortcomings of these models. WGNE has recently launched a model inter-comparison aimed at improving the understanding of aerosol impacts on numerical weather prediction. Three case studies were proposed to the participants: a severe anthropogenic pollution case in January 2013 in Northern China, a biomass-burning event in Brazil in September 2012 and a dust storm over Egypt on 18 April 2012. This paper focuses on the dust episode of 18 April 2012 over the Eastern Mediterranean. Another dust storm, which took place on 12 and 13 April 2012 in the Central Sahara region was also studied, as more ground observations were available.

2 Dust episodes of April 2012 in the Sahara and Eastern Mediterranean

2.1 Available observations

Surface observations of meteorological parameters in Algeria and Egypt were used to analyze the meteorological situation. Observations were not available over Libya because of the political situation in this period. Daily weather charts from the Berlin University and the UK Met Office were also used to assess the synoptic evolution of the dust storm. Observations are much sparser for radiative fluxes than for meteorological parameters. The Baseline Surface Radiation Network (BSRN) (Heimo et al., 1993) maintains two stations in the area of interest: Tamanrasset (Mimouni, 2013 in Southern Algeria and Sede Boqer in Israel, Lyubansky, 2012). Unfortunately, observations from Sede Boqer were not available in April 2012. Downwelling surface flux of shortwave and long-wave radiation at Tamanrasset, in Southern Algeria, were measured with a frequency of 1 min. A climatology of daily downward surface solar flux has been established by Satellite Application Facility on Climate Monitoring (CM-SAF, Stengel et al., 2013), derived from remote sensing by the Spinning Enhanced Visible and Infrared Imager (SEVIRI) sensor onboard MeteoSat Second Generation (MSG), with an accuracy of 20 W m^{-2} . Finally AOD observations were available from the AEROSOL ROBOTICS NETWORK (AERONET, Holben et al., 1998) of ground observations. The sta-

Title Page

Abstract

Introduction

Conclusions

References

Tables

Figures



Back

Close

Full Screen / Esc

Printer-friendly Version

Interactive Discussion



tions used in this study are Tamanrasset, collocated with radiative fluxes observation from BSRN, and Cairo in Egypt. As these observations are provided by sun photometers, they are available only during the day. To supplement the absence of AOD observations at some stations, simulated AOD was also plotted to provide a qualitative assessment of the presence of dust aerosols. Total AOD observations are also available from MODIS over desert areas, using the Deep Blue algorithm (Shi et al., 2013).

2.2 Sahara dust storms of April 2012: synoptic evolution

Dust storms are a frequent occurrence in the Sahara, where dust aerosol production areas are widespread. As the soil is generally very dry in these regions and predominantly composed of sand, surface temperatures can reach very high values in April. Higher altitude colder air from Mediterranean lows occasionally affects the area. The severe dust storm that affected Libya, Egypt and most of the Eastern Mediterranean basin on 17–18 April 2012 was produced by the conjunction of a deep low circulating over the Mediterranean and of a heat low that originated over Western Libya–Eastern Tunisia on 16 April 2012, caused by very high temperatures over the desert areas that dominate this area. Figure 1 shows mean sea-level pressure analyses over Northern Sahara and Southern Mediterranean from 17 to 19 April 2012. The merging and interaction of the heat low caused by high surface temperatures over desert areas and the Mediterranean low that is associated with mid-tropospheric colder air is clearly shown. This interaction, and the development of a powerful anticyclone over the central Sahara, led to the rapid deepening of a low between Crete and Greece on 18 April. The heat low moved in a North-Easterly direction, left Western Egypt in the night of 17 to 18 April, and was then absorbed by the larger and fast moving Mediterranean low, which then moved quickly towards the North on 19 April 2012.

The synoptic situation led to high and sustained winds on 17–18 of April over North-east Libya and Egypt, reaching 11 to 14 ms⁻¹ for more than 24 h, according to model forecasts and observations. This led to the suspension of a very high load of dust aerosols, with AOD reaching 4.5 in Cairo at noon on 18 April. The interaction between



Positive feedback of dust aerosol

S. Remy et al.

[Title Page](#)[Abstract](#)[Introduction](#)[Conclusions](#)[References](#)[Tables](#)[Figures](#)[⏪](#)[⏩](#)[◀](#)[▶](#)[Back](#)[Close](#)[Full Screen / Esc](#)[Printer-friendly Version](#)[Interactive Discussion](#)

dust aerosols and the synoptic situation is shown by Fig. 2, which shows daily AOD over Eastern Sahara from the Deep Blue algorithm applied to MODIS/Aqua observations. The large dust aerosol load created by the heat low was then advected Northwards by the deep Mediterranean low, towards Israel, Turkey and the Eastern Mediterranean on 18–19 April 2012.

This dust storm was preceded by another event between 11 and 15 April 2012, that affected the central Sahara up to Libya and Western Egypt. This was caused by a persistent and slow moving heat low over central Sahara combined with a deep low over Western-central Mediterranean. This event was also studied as the whole of April 2012 was forecasted by the global MACC-II system in the framework of the WGNE model inter-comparison. This allowed comparing forecasts of radiative fluxes against ground observations at Tamanrasset (Algeria), which was affected by the dust storm of 11 to 15 April but not by the following storm of 17–18 April 2012.

2.3 Impact on observed radiative fluxes at the surface

The very high load of dust that was observed on 17–18 April 2012 had pronounced impacts on the radiative fluxes at the surface. Figure 3 shows a daily average of downward surface solar flux (DSSF) on 17–18 April 2012. Satellite imagery from MODIS (not shown) indicates that clouds were nearly entirely absent from the parts of Libya and Egypt that were affected by the dust storm. The difference of more than 100 W m^{-2} in DSSF between Eastern Libya and its surroundings on the 17 April, and between Northern Egypt and its surroundings on 18 April corresponds thus entirely to the radiative forcing from dust particles in the shortwave spectrum.

Figure 3 shows a time-serie of surface downward long-wave and shortwave radiative fluxes at the surface, together with cloud cover, 2 m temperature and AOD at Tamanrasset. Shortwave radiation is decomposed into direct and total, which allows to deduce the diffuse component of incoming solar radiation, as the difference between the two. Tamanrasset was mostly affected by the dust storm from 12 to 14 April. High clouds were also present from 10 to 13 April. Therefore it is hard to distinguish their effect

Positive feedback of dust aerosol

S. Remy et al.

Title Page

Abstract

Introduction

Conclusions

References

Tables

Figures

I◀

▶I

◀

▶

Back

Close

Full Screen / Esc

Printer-friendly Version

Interactive Discussion



from the radiative impact of clouds and aerosols during this period. Observations at Tamanrasset show that when clouds and aerosols are present, the diffuse component of incoming solar radiation is increased whereas direct solar radiation is nearly halved: maximal total solar radiation is 200 to 300 W m⁻² smaller from 11 to 13 April compared to 14 to 18 April. The diurnal cycle of temperature on these days is also less pronounced, which could have been caused by both aerosols and clouds. Downward long-wave fluxes at the surface are on average around 60 W m⁻² higher from 11 to 13 April compared to 14 to 18 April. As the observed clouds are mainly high clouds, which have little effect on the downward long-wave flux at the surface, it is likely that this difference is caused by the presence of dust particles from 11 to 14 April. Also, high clouds were observed on the night of 17 to 18 April, but the dust aerosol load was small these two days. The impact on long-wave radiation fluxes was small, which confirms that high clouds don't cause an increase in downward long-wave fluxes at the surface. This shows that the radiative forcing in the long-wave spectrum from 11 to 13 April is mostly caused by the presence of dust particles.

3 Methodology

The objective of this study is to assess the impact of the aerosol direct effect on the forecasted meteorological parameters during the dust storms that affected the Sahara and Eastern Mediterranean basin in April 2012. To achieve that, the MACC-II global system was run with the aerosol direct effect estimated from a climatology or from prognostic aerosols, with various configurations. All runs were carried out with a T_L511 horizontal spectral resolution which corresponds to a grid-box size of about 40 km. 60 vertical hybrid sigma-pressure levels were used, the lowest level being 17 m above the surface.

3.1 Cycling forecasts

In this configuration, the model is run without assimilating AOD. The meteorological fields are initialised from the global MACC-II analysis, and the aerosol fields were initialised from the MACC re-analysis on the 10 April 2012 only and otherwise from the previous 24 h forecast. In this configuration the aerosol fields are not constrained by any observations and could drift away from observed values.

The main advantage of this configuration comes from comparing the model outputs with and without radiatively interactive aerosols. Since the meteorological analyses are the same for all the experiments, the differences between the meteorological forecasts originate only from the way interaction between aerosols and radiation are computed, i.e. using prognostic aerosols or a climatology. Cycling forecasts are thus adequate to assess the aerosols' impact on forecasted meteorological fields.

A default for this configuration is that since the meteorological analysis comes from another experiment, the interaction between aerosols and meteorology is reset at every forecasting cycle. Experiments were carried out with both aerosols and meteorological fields initialised from the previous 24 h forecast, and they showed the same results qualitatively than when meteorological fields were initialised from the global MACC-II analysis. The amplitude of the aerosol-meteorology interaction was however significantly larger since it was also included in the meteorological analysis.

Cycling forecasts were carried out for the period from 10 to 30 April 2012, every 24 h, with runs starting at 00:00 UTC. July 2012 was also run, in order to check if the conclusions reached for April 2012 are also valid globally for other periods of time.

3.2 Shortwave and long-wave aerosol direct impact

Since the physical phenomena that underlie the aerosol direct effect are not the same in the shortwave and in the long-wave spectra, these two contributions can be separated in the MACC-II global system. It is now possible to compute the total radiative impacts of aerosols, using prognostic aerosols in the shortwave spectrum and the

Title Page

Abstract

Introduction

Conclusions

References

Tables

Figures



Back

Close

Full Screen / Esc

Printer-friendly Version

Interactive Discussion



aerosol climatology of Tegen et al. (1997) in the long-wave spectrum, and vice-versa. As a consequence, it is possible now to decompose the prognostic aerosol direct effect (or “Total aerosol effect”) in its “Shortwave aerosol direct effect” and “long-wave aerosol direct effect” components.

- 5 The following experiments were carried out with cycling forecasts:
- REF: reference experiment with the aerosol direct effect computed from an aerosol climatology,
 - LW: the long-wave component of the aerosol direct effect is computed using prognostic aerosols, the shortwave part is computed with an aerosol climatology,
 - 10 – SW: the shortwave component of the aerosol direct effect is computed using prognostic aerosols, the long-wave part is computed with an aerosol climatology,
 - TOTAL: both the shortwave and the long-wave components of the aerosol direct effect are computed using prognostic aerosols.

3.3 Assimilation runs

15 In this configuration the model is run with the full 4D-Var data assimilation, providing initial conditions for both the aerosol and meteorological variables. The following experiments were carried out with assimilation runs:

- REF_ASSIM: reference experiment with the aerosol direct effect computed from an aerosol climatology,
- 20 – TOTAL_ASSIM: the aerosol direct effect is computed using prognostic aerosols.

Runs were carried out at 00:00 and 12:00 UTC every day for the whole of April 2012, with an assimilation window of 12 h. However, only the runs of 00:00 UTC go beyond 12 h of forecast time. As a follow-up to cycling forecasts, assimilation runs will allow to study how differences in the model affect initial conditions through the data assimilation.

Positive feedback of dust aerosol

S. Remy et al.

Title Page

Abstract

Introduction

Conclusions

References

Tables

Figures



Back

Close

Full Screen / Esc

Printer-friendly Version

Interactive Discussion



4 Results of the cycling forecasts runs at Cairo and Tamanrasset

Forecasts of the REF, SW, LW and TOTAL experiments are evaluated against ground and remote observations of meteorological and radiative parameters, using bias and Root Mean Square Error (RMSE) scores. The period of study is from 10 to 20 April 2012. A detailed analysis is carried out for Cairo and Tamanrasset. General scores over the Sahara and Mediterranean will be presented in the following section.

4.1 Shortwave aerosol direct effect

Figure 4 shows observed and forecasted parameters at Cairo and Tamanrasset for experiments REF and SW.

4.1.1 Results in Cairo

On 18 April, the forecasted AOD reached 3: the predicted dust aerosol load was much larger than the Tegen climatology, which gives values of 0.3 to 0.4 (Tegen et al., 1997). As a consequence, the aerosol direct effect on the shortwave spectrum was much more intense also: the peak of incoming solar radiation on 18 April was forecasted to be nearly 400 W m^{-2} smaller for the SW experiment. It is interesting to note that the incoming solar radiation can be larger for SW compared to REF, as occurred on 16 and 17 April, when predicted aerosol load was very small (0.1 to 0.2) than the values given by the monthly climatology of Tegen et al. (1997). For these two days, the radiative forcing computed with prognostic aerosols was actually smaller than the one computed using the climatological values.

Downwelling long-wave radiation at the surface is also different on 18 April; it is around 10 W m^{-2} smaller for the SW experiment. This difference can be explained by the difference in lower atmosphere temperatures, which controls long-wave radiative transfer.

Title Page

Abstract

Introduction

Conclusions

References

Tables

Figures



Back

Close

Full Screen / Esc

Printer-friendly Version

Interactive Discussion



Positive feedback of dust aerosol

S. Remy et al.

[Title Page](#)[Abstract](#)[Introduction](#)[Conclusions](#)[References](#)[Tables](#)[Figures](#)[Back](#)[Close](#)[Full Screen / Esc](#)[Printer-friendly Version](#)[Interactive Discussion](#)

This strong radiative forcing influences maximum temperatures on 18 April: they are 3 to 4 °C lower for the SW experiment. As the reference experiment had already a negative bias of around 1 °C for this period, the bias and also RMSE increased for Cairo in SW. Associated with this impact on temperature is an impact on wind speed. On 18 April, wind speed during day-time is 1 to 1.5 m s⁻¹ smaller with the SW experiment. This can be explained by the fact that with lower maximum temperatures the PBL is less unstable; as a consequence the wind profile associated with the thermal stratification tends to be more logarithmic and surface winds tend to be weaker. For surface winds, the scores are identical between SW and REF.

Expectedly, AOD itself is overall slightly smaller for SW because of less wind blown dust emissions. Values are lower for SW on the morning of 18 April.

4.1.2 Results in Tamanrasset

In Tamanrasset, the qualitative behavior is the same as in Cairo, but the differences between SW and REF are smaller, as the aerosol load on 12–13 April in Tamanrasset was smaller than on 18 April in Cairo. The incoming solar radiation at the surface is closer to observations with SW compared to REF: the positive bias is slightly reduced, and RMSE is also lower. As in Cairo, the AOD is a bit smaller with SW compared to REF.

4.2 Long-wave aerosol direct effect

Figure 5 shows observed and forecasted parameters at Cairo and Tamanrasset for experiments REF and LW.

4.2.1 Results in Cairo

The impact of the prognostic aerosols direct effect is very important on the downwelling long-wave radiation at the surface; its values are on average 30 W m⁻² larger for the LW experiments compared to REF for the whole period. On 18 April, the difference is

Positive feedback of dust aerosol

S. Remy et al.

[Title Page](#)[Abstract](#)[Introduction](#)[Conclusions](#)[References](#)[Tables](#)[Figures](#)[◀](#)[▶](#)[◀](#)[▶](#)[Back](#)[Close](#)[Full Screen / Esc](#)[Printer-friendly Version](#)[Interactive Discussion](#)

nearly 100 W m^{-2} . While the incoming solar radiation was affected by the SW experiment only when the AOD was highest, i.e. on 18 April, long-wave radiation in the LW experiment is more sensitive to lower values of AOD. The incoming solar radiation is nearly unchanged every day.

The radiative forcing from the aerosols in the long-wave spectrum has a strong impact on minimum temperatures from 13 to 20 April. They are higher by up to $3\text{--}4^\circ\text{C}$ with the LW experiment. Because of higher night-time temperatures and similar incoming solar radiation between the REF and LW experiments, day-time temperatures are also higher, by up to 2°C on 19 April. As a consequence of this influence of higher long-wave radiation on both minimum and maximum temperature, the negative bias of the REF experiment for 2 m temperatures disappears entirely with the LW experiment, and the RMSE is also reduced.

As a consequence of higher temperatures at the surface, lower atmosphere thermal stratification is more unstable during the day, and less stable during the night. This brings higher winds, mainly during day-time, caused by higher thermal production of turbulence. The negative bias of the REF experiment for 10 m wind speed is slightly smaller for the LW experiment, with unchanged RMSE.

When AOD values are above 0.5, AOD is systemically and significantly higher for the LW experiment compared to REF, with an average that is more than 10 % larger for LW compared to REF. As the AOD peak of the 18 April is generally underestimated, this reduces the difference between forecasts and observations on that day. On 15 April on the other hand, model AOD is larger than observations; values from the LW experiment are then a bit farther away from observations. This increase in AOD in the LW experiment as compared to REF is linked to the associated increase in wind speed. This feedback will be explained in more detail in Sect. 6.

4.2.2 Results in Tamanrasset

Similarly to Cairo, the downwelling long-wave fluxes at the surface are significantly increased by the LW experiment compared to the REF experiment. This completely cancels the negative bias of REF for this parameter: LW actually shows a small positive bias. RMSE is unchanged between the two experiments. As in Cairo, the direct effect is much more sensitive to an increased dust aerosol load in the long-wave spectrum than in the shortwave. While in the shortwave, relatively high values of AOD are needed to make a difference, in the long-wave even relatively small values can make a difference in the radiative impact of aerosols. In the long-wave spectrum, larger dust particles, which don't contribute as much as small dust particles to AOD, play a more important role whereas in the short-wave spectrum, smaller particles are more efficient in absorbing or scattering the incoming solar radiation. This is especially clear on 19 and 20 April, with AOD of around 0.5–0.8. The difference in downwelling long-wave fluxes at the surface between REF and LW reaches more than 50 W m^{-2} , while the difference in incoming solar radiation between REF and SW was small: 1 W m^{-2} on average.

2 m temperatures are much higher during night-time when AOD is relatively large, by up to $2\text{--}3^\circ\text{C}$. Day-time temperatures were slightly higher on days most affected by the dust storm, identical otherwise. As in Cairo, the 2 m temperature negative bias of REF is completely canceled in the LW experiment, even though RMSE is nearly unchanged.

10 m wind speed is slightly larger with the LW experiment compared to REF, associated with generally slightly larger AOD.

4.3 Total aerosol direct effect

Figure 6 shows observed and forecasted parameters at Cairo and Tamanrasset for experiments REF and TOTAL. The impact of interactive aerosols radiative effect on radiative fluxes for TOTAL is not merely the sum of SW and LW: for the long-wave radiative fluxes, the difference between TOTAL and REF is slightly smaller than the dif-

[Title Page](#)[Abstract](#)[Introduction](#)[Conclusions](#)[References](#)[Tables](#)[Figures](#)[Back](#)[Close](#)[Full Screen / Esc](#)[Printer-friendly Version](#)[Interactive Discussion](#)

Positive feedback of dust aerosol

S. Remy et al.

[Title Page](#)[Abstract](#)[Introduction](#)[Conclusions](#)[References](#)[Tables](#)[Figures](#)[Back](#)[Close](#)[Full Screen / Esc](#)[Printer-friendly Version](#)[Interactive Discussion](#)

ference between LW and REF whereas for the shortwave radiative fluxes the difference between TOTAL and REF is larger. This can be explained by the fact that the impact of interactive aerosols on the long-wave spectrum is associated with higher dust AOD, this higher amount of aerosols in return enhances the impact of the aerosol direct effect on the shortwave spectrum. The impact of TOTAL on temperature and AOD are close to the one of LW, only slightly smaller. This indicates that the radiative effect of aerosols in the long-wave spectrum appear to have more impact on surface meteorological parameters than the effect on the shortwave spectrum in this case.

For Cairo, taking into account prognostic aerosols direct effect clearly has a positive impact on temperatures, with a significant reduction of both bias and RMSE. For Tamanrasset, the negative bias of temperatures of REF is cancelled by TOTAL, without much effect on the RMSE. The impact on 10 m wind speed appears to be small for both stations. The BSRN observations at Tamanrasset indicate that the TOTAL experiment is closer to observations of long-wave and shortwave radiative fluxes than the REF experiments.

4.4 Forecasts at day + 1

Figure 7 shows the same plots as Fig. 6 for forecast times of 24 to 45 h instead of 3 to 24 h. Overall, the conclusions are the same for forecasts at day + 1 as for forecasts at day + 0: improved radiative fluxes produce better forecasts of 2 m temperatures, at Cairo and Tamanrasset. The impact on dust AOD appears slightly larger at day + 1 than at day + 0. Associated with that, daytime maxima of shortwave radiative fluxes are smaller for the TOTAL experiment at day + 1 compared to day + 0.

5 Interaction of shortwave and long-wave aerosol radiative impact

Comparisons of the REF, SW, LW and TOTAL experiments at selected locations indicated that the radiative effect of dust AOD impacts temperatures through the short-

Positive feedback of dust aerosol

S. Remy et al.

Title Page

Abstract

Introduction

Conclusions

References

Tables

Figures



Back

Close

Full Screen / Esc

Printer-friendly Version

Interactive Discussion



5 wave and long-wave radiative fluxes, but also dust AOD itself. This section aims to understand how the direct effects impacts meteorological processes and then how in return these processes impact dust AOD. First, the interaction of shortwave and long-wave aerosol direct effect will be studied. The forecast starting on 17 April 2012 at 00:00 UTC will be used for that, forecast times between 24 h (local night-time) and 36 h (local day-time).

10 The results from Sect. 4 showed that the radiative impact of aerosols on the whole spectrum is different from the sum of radiative impacts on shortwave and long-wave spectra. Figure 9 shows the difference in dust AOD between REF and SW, LW and TOTAL, and then the difference between the average of SW and LW on one hand, and TOTAL on the other hand. Figure 8 shows the dust AOD forecasted by the REF and TOTAL experiment for the same base time and forecast times 24 and 36 h. It allows us to compare the location of the dust aerosol layer and of the regions where dust AOD is most impacted by the aerosol radiative effects. The LW experiments show generally 15 much higher AOD as compared to REF; the regions where dust AOD is up to 1–1.5 larger for LW corresponds to the regions where AOD is the highest. The difference is more important at 24 h forecast time than at 36 h. A small band of smaller values of dust AOD for the REF experiment lies in front of the dust storm: the dipole there indicates that the front that is moving from West to East, associated with the dust storm, is forecasted to move slower with the LW experiments. This shows that the aerosol direct effect on the long-wave spectrum impacts the synoptic situation that causes the dust storm. The band of lower values of dust AOD for the LW experiments is wider at 36 h 20 forecast time: this indicates that the impact of the aerosol direct effect on the position of the front increases with forecast time.

25 The comparison of the SW and REF experiments shows nearly opposite patterns: dust AOD is generally lower with the SW experiments; however a positive-negative dipole at the location of the front indicates that its position is forecasted further East with the SW experiment compared to REF. Again, this difference in front position forecast between REF and SW widens with forecast time. The generally positive difference

between REF and SW is smaller in amplitude compared to the negative difference between REF and LW. These tendencies match the conclusions of Sect. 4.

The difference between REF and TOTAL indicates that TOTAL, like LW, is generally above REF in terms of dust AOD at forecast times 24 and 36 h. The same patterns as for LW are found but attenuated: this confirms the conclusions of Sect. 4, i.e. that the contribution of the aerosol direct effect on the long-wave spectrum more than compensates the contribution on the shortwave spectrum in this situation, even though the long-wave radiative effect enhances the shortwave radiative effect through an increased load of dust aerosols. Comparing this plot against the difference between REF and the average of SW and LW shows that TOTAL is more skewed towards LW than the average of LW and SW. This could be because the maximum load of aerosols occur during the night of 17 to 18 April 2012, and decreases rapidly during the morning of 18 April, as shown by Fig. 8. The same conclusions can be drawn from Table 1, which gives the average dust AOD value over July 2012 for the REF, SW, LW and TOTAL experiments. Again, TOTAL is much closer to LW than to the average of LW and SW.

This behavior can be explained by the fact that SW impacts meteorological processes only during the day, as shown clearly by Fig. 4, whereas LW impacts surface temperature during the day and at night. In the TOTAL experiment, the lower maximum temperatures caused by the shortwave aerosol effect are canceled out by the higher maximum temperatures due to the long-wave aerosol effect; however minimum temperatures remain higher as the shortwave aerosol effect does not impact them. This also explains why TOTAL is closer to LW during the night, at 24 h forecast time, than during the day, at 36 h forecast time, though this could also be due to the decreasing aerosol load as well.

6 Mechanism of the aerosol – boundary layer meteorology feedback

The previous sections showed that on one hand, long-wave aerosol radiative impact is associated with much higher amounts of dust aerosols, on the other hand that the

Positive feedback of dust aerosol

S. Remy et al.

Title Page

Abstract

Introduction

Conclusions

References

Tables

Figures



Back

Close

Full Screen / Esc

Printer-friendly Version

Interactive Discussion



shortwave aerosol radiative impact brings smaller amount of dust aerosols. In this section we are going to concentrate on the interaction of meteorological processes on the dust aerosol load in the TOTAL experiment.

6.1 Impact of the boundary layer meteorological processes on dust aerosol load

Meteorological processes can impact the dust aerosol load through the sources and the sinks. As there was no rain or clouds over Libya and Egypt on 17–18 April 2012, scavenging is of no relevance here. Sedimentation is applied only to the largest dust aerosol bin and was a very small sink for this bin compared to dry deposition. Dry deposition processes are parameterized as a function of dust aerosol concentration in the lowest model level. Associated with the higher dust AOD of TOTAL compared to REF was a higher content of aerosols for the three bins in the lowest model level, and dry deposition as a consequence was larger for TOTAL than for REF. A reduction in the dust aerosol sinks is thus not the cause of the higher aerosol load of TOTAL.

Figure 10 shows the difference REF – TOTAL for dust aerosol production and wind speed at 10 m. Dust aerosol production and winds are generally larger for TOTAL than for REF over land, the difference being more important during the night (24 h forecast time) than during the day (36 h forecast time). The only places where dust aerosol production and winds are smaller correspond to the front, which was forecasted to move slightly slower with TOTAL compared to REF. Higher amounts of dust aerosols for TOTAL are thus a consequence of stronger winds. Stronger winds can be caused by a combination of two factors:

- Synoptic causes: the pressure gradient and geostrophic component of winds could be larger,
- Local causes: a different thermal stratification of the boundary layer modifies the vertical structure of the winds in the boundary layer.

Positive feedback of dust aerosol

S. Remy et al.

Title Page

Abstract

Introduction

Conclusions

References

Tables

Figures



Back

Close

Full Screen / Esc

Printer-friendly Version

Interactive Discussion



As the initial conditions for meteorological parameters are identical between REF and TOTAL, and since the only difference in the forward model concerns the use of prognostic aerosols for the computation of the aerosol radiative effect, stronger winds for the TOTAL experiments are a consequence of the higher dust aerosol amounts.

5 The meteorological phenomena involved in this process will be detailed in the next two subsections.

6.2 Impact of the dust aerosol on large scale meteorological processes

In this subsection the respective contributions of synoptic winds and different thermal stratification to the wind speed increase of TOTAL compared to REF are studied. Figure 11 shows the difference between REF and TOTAL for mean sea-level pressure and wind speeds at 925 hPa. Wind speeds at 925 hPa are less influenced by surface properties and should be more representative of the large-scale component of wind speed. The pressure difference plots can be compared against Fig. 1; they show that the pressure is slightly lower at the bottom of the area of low pressure that crosses Egypt from West to East during the night and morning of 18 April. The difference reaches 1 to 1.5 hPa and appears to be increasing in area with forecast time. The areas where pressure is lower in the TOTAL experiments are closely collocated with the areas where temperature at 850 hPa is higher with TOTAL, as shown by Fig. 12 on the right hand side. This seems to indicate that the cause of lower pressures for TOTAL are warmer temperatures over most of the boundary layer.

20 These areas of lower pressure for TOTAL (and higher pressure gradients) are however more restricted than the areas where surface winds are stronger for TOTAL, as shown on Fig. 10. Winds at 925 hPa also show a generally smaller difference between TOTAL and REF than for wind speeds at 10 m at night. The areas where the differences in 925 hPa winds are the highest correspond to areas where the pressure differences are the most important, which confirm that 925 hPa winds are a good marker of the synoptic winds. It appears then that the large scale winds are the most important con-

Positive feedback of dust aerosol

S. Remy et al.

Title Page

Abstract

Introduction

Conclusions

References

Tables

Figures



Back

Close

Full Screen / Esc

Printer-friendly Version

Interactive Discussion



tributor to wind speed differences at 10 m during the day, but that it is not the dominant source of wind increase at night.

Large scale wind speeds are also affected above the PBL. Figure 14 shows profiles of wind speed, total dust aerosol mixing ratio and temperature on 18 April 2012 at 00:00 UTC, at a point that lies at 22.5° N, 22° E, just before the front crosses that area. Mid-troposphere winds are overall weaker in the TOTAL experiment, which explains why the front moves slightly slower, as noted before. These changes in synoptic winds are driven by the large change in thermal stratification in the boundary-layer, caused by the dust aerosol layer.

6.3 Impact of the dust aerosol on boundary layer meteorological processes

6.3.1 Night-time processes

Figure 12 shows differences in 2 m temperature and 850 hPa temperatures. At night, driven by much higher downwelling long-wave fluxes, 2 m temperatures are much higher for TOTAL over a large area over land, while the 850 hPa temperatures differences are much more localized and show less amplitude. Over the sea, the differences are much smaller, as the heat capacity of water is much larger than that of the mostly sandy soils of the region. The areas where temperature at 850 hPa is significantly higher with TOTAL are well collocated to the areas where the dust aerosol mixing ratio is higher for TOTAL (not shown): the increase in temperature is caused by thermal radiation of the aerosol layer. As a consequence of these much higher surface temperatures, the lower atmosphere is less stable with TOTAL compared to REF during the night, which means that wind profiles should get closer to the linear profile that is typical of neutral boundary layers instead of the logarithmic profile that is typical of a stable boundary layer.

Figure 13 helps to refine this diagnosis: it shows the time evolution of forecasted dust AOD, temperature gradient between 2 m and 850 hPa, sensible heat flux at the surface and 10 m wind speed, at a point that lies at 22.5° N, 22° E, in the midst of the region

Title Page

Abstract

Introduction

Conclusions

References

Tables

Figures



Back

Close

Full Screen / Esc

Printer-friendly Version

Interactive Discussion



Positive feedback of dust aerosol

S. Remy et al.

Title Page

Abstract

Introduction

Conclusions

References

Tables

Figures



Back

Close

Full Screen / Esc

Printer-friendly Version

Interactive Discussion



where the temperature is much higher at 2 m for TOTAL, and slightly lower at 850 hPa. The increase in dust AOD with prognostic aerosols direct effect is clearly visible. During the day, thermal stratification is not much impacted; however at night the impact of the dust aerosol layer on thermal stratification is very pronounced when AOD is above 0.5–0.7. While in REF 2 m and 850 hPa are more or less equal at night, in TOTAL, 2 m temperature is 3 to 5 K higher than 850 hPa temperature at night. This has a very significant impact on surface sensible heat flux: while these fluxes are slightly positive, i.e. the surface is losing heat, in REF, they are close to zero for TOTAL. When AOD is maximum, early in the morning of 18 April, the sensible heat flux is even negative instead of positive: the surface is actually gaining heat. When dust AOD is high, the sensible heat flux is reduced during the day for TOTAL compared to REF, as the solar flux is absorbed or diffused by the aerosol layer. This occurs on 18 April and also, on a smaller scale, on 15 April. There is a clear correlation between the sensible heat flux at the surface and wind speed at 10 m: when sensible heat flux is lower at night for TOTAL, wind speed at 10 m is higher: as the most important differences in surface heat flux occur during the early mornings of 15 and 18 April and during the night of 16 to 17 April, wind speeds at 10 m are also significantly higher for TOTAL at the same times.

The vertical structure of the changes brought by TOTAL compared to REF are shown in the dust aerosol mixing ratio, wind and temperature profiles of Fig. 14. While 10 m wind speed is significantly higher with TOTAL, the low-level jet, a typical feature of stable boundary layers with temperature inversions (Banta et al., 2002), is weaker and higher with TOTAL. Stronger winds in the lower PBL causes more turbulent mixing, which causes lower temperatures for TOTAL compared to REF above 950 hPa at this location. It is also interesting to note that the increase in AOD brought by TOTAL compared to REF is caused by an increase in the aerosol load between 925 and 800 hPa; at the surface the mixing ratio is actually slightly lower for TOTAL.

6.3.2 Daytime processes

Figure 12 shows that during the day, the differences in 2 m and 850 hPa temperatures are much better collocated than during the night over land. Over the land, temperatures are generally higher for TOTAL, by up to 3–4 K at the surface and up to 2 K at 850 hPa.

5 Over the sea, temperatures are lower for TOTAL, at 2 m and 850 hPa, by 0.1 to 0.5 K. The radiative impact of aerosols on the shortwave spectrum is more prominent over the sea: unlike over land, it is not compensated by the impact of aerosols on the long-wave spectrum.

Figure 15 shows the same time evolution as Fig. 14, at a point located at 31° N, 32° E, where the dust storm peaked shortly before noon on 18 April. The link between dust AOD, thermal stratification of the PBL, sensible heat flux and wind speed is similar to what was shown in Fig. 14 from 14 to 17 April. However, on the afternoon of 18 April, the temperature gradient was smaller for TOTAL, as 2 m temperatures were lower. Associated with lower surface temperatures was a lower sensible heat flux during daytime on 18 April. This occurred because the maximum values for AOD were forecasted during daytime at this location, and were very much higher compared to values during the night of 17 to 18 April. The high values of AOD during day-time were associated with reduced incoming solar radiation, which was enough to offset the higher minimal temperatures for TOTAL to lower maximum temperatures. This shows that the timing of the onset of the storm has a strong influence on how the dust aerosol load impacts meteorological processes.

Figure 16 shows the vertical profiles of dust AOD mixing ratio, temperature and wind speed on 18 April 2012 at 12:00 UTC at the same point. The aerosol layer, advected from the South-West, is rather high, with a maximum between 850 and 700 hPa. While the mixing ratio is much higher there for TOTAL, which explains the higher values for AOD, below 900 hPa, dust aerosol mixing ratio is actually lower for TOTAL. The temperature gradient is very high for both experiments, as a much colder air mass was advected over the region just behind the front: 850 hPa temperature dropped 12 to

Title Page

Abstract

Introduction

Conclusions

References

Tables

Figures



Back

Close

Full Screen / Esc

Printer-friendly Version

Interactive Discussion



13°C in the few hours before 12:00 UTC. As the skies are mostly clear and because soil is mostly sandy in this area, daytime warming of the surface is very important for both experiments. Temperatures below the aerosol layer are lower for TOTAL, as the incoming solar radiation is partly absorbed or diffused by the aerosols. This large amount of solar energy that is diffused or re-emitted by the aerosols explain why temperatures are significantly higher there for TOTAL: a small inversion is forecasted around 900 hPa. Associated with this inversion, TOTAL forecasts a low-level jet whereas REF does not. In the absence of daytime radio-sonde data in Egypt, it is hard to verify whether this low-level jet was observed or not. The closest daytime radio-sonde data available is at Tel-Aviv, in Israel, and a low level jet with a maximum between 900 and 850 hPa, associated with a temperature inversion was indeed observed there on 18 April at 12:00 UTC. As shown on Fig. 6, values of dust AOD forecasted in Tel-Aviv at this time were between 1.5 and 2: it is highly probably that the dust aerosol layer was the cause of this daytime inversion and low-level jet at Tel-Aviv.

7 Assimilation runs

Cycling forecasts showed a mainly positive feedback between boundary layer meteorological processes and dust aerosols. Figure 17 shows the differences between the experiments REF_ASSIM and TOTAL_ASSIM for dust AOD, 10 m wind speed, 2 m temperature and mean sea-level pressure, for the runs starting at 00:00 UTC on 17 April 2012. This figure can be compared to Figs. 9–12 which shows the same differences for REF and TOTAL. This comparison shows that the interaction between boundary layer meteorology and dust aerosols is more pronounced with assimilation runs: the difference in dust AOD is larger between TOTAL_ASSIM and REF_ASSIM compared to between TOTAL and REF, at day or night. This larger increase of dust AOD with assimilation runs is caused by larger differences in wind speeds, itself caused by larger pressure and surface temperature differences.

Positive feedback of dust aerosol

S. Remy et al.

Title Page

Abstract

Introduction

Conclusions

References

Tables

Figures



Back

Close

Full Screen / Esc

Printer-friendly Version

Interactive Discussion



Positive feedback of dust aerosol

S. Remy et al.

[Title Page](#)[Abstract](#)[Introduction](#)[Conclusions](#)[References](#)[Tables](#)[Figures](#)[Back](#)[Close](#)[Full Screen / Esc](#)[Printer-friendly Version](#)[Interactive Discussion](#)

This behavior of TOTAL_ASSIM can be explained by the fact the initial conditions of meteorological parameters already contain (unlike TOTAL) the impact of dust aerosol-meteorology interaction, through the first guess. As such, it is expected that the trends of TOTAL compared to REF, that occur only in the forecast stage, are amplified for TOTAL_ASSIM compared to REF_ASSIM. As the dust storm of 17–18 April 2012 occurs in a location where both meteorological and total AOD observations are sparse, the first guess has comparatively more weight in the initial conditions in this situation.

7.1 Impact on the quality of temperature and AOD forecasts by the MACC global system

The previous sections showed that surface temperature and AOD are significantly affected by how the aerosol radiative effect is computed. This sections aims to assess whether using prognostic aerosols to compute the aerosol radiative effect is beneficial for the forecasts of these two parameters. As assimilation runs are considered, the configuration is very close to that of the Near Real Time global MACC-II system.

7.1.1 Temperature forecasts

Temperature forecasts of TOTAL_ASSIM are evaluated against observations for several stations in Egypt. As the resolution was rather crude, several stations were not taken into account because of land–sea representativity problems. Figures 6 and 7 showed that using prognostic aerosols has a beneficial impact on temperature forecasts with cycling experiments: a negative bias on minimum temperatures is removed and RMSE is decreased. These results were achieved at two different stations that were affected by two different storms. In this section a more general approach is followed: forecasts are evaluated for the period from 10 to 25 April 2012, over the whole of Egypt, for runs starting at 00:00 UTC. Only REF_ASSIM and TOTAL_ASSIM will be assessed as they correspond to the operational setup of the MACC global system.

The evaluation will be carried out for 2 m temperature because it is the meteorological parameter that was the most impacted by the interactive aerosols radiative effect.

Tables 2 and 3 show the RMSE and bias of the REF_ASSIM and TOTAL_ASSIM, over a selection of stations in Egypt and Israel, for forecast times ranging from 3 to 36 h.

3 h forecasts are considerably improved in terms of RMSE, showing that with assimilation runs, the impact of using prognostic aerosols radiative effect is important for the analysis and for short-term forecasts. The fact that there are not many observations to be used in the assimilation system in the Sahara region probably explains partly why the impact of the first guess is so large in the initial conditions for these simulations. Improvements in RMSE are most significant inland, in the desert and in the Nile Valley. This large improvement in RMSE for TOTAL_ASSIM is due to the near-canceling of an important cold bias at night: for 3 h forecasts, the average bias over selected stations is reduced from -1.2 to -0.2 K. 3 h forecasts of TOTAL_ASSIM are warmer everywhere; the station with the highest difference is Siwa, which lies in the desert in Western Egypt. Coastal stations with a small warm bias with REF_ASSIM see this bias increased with TOTAL_ASSIM. Overall, the behavior is consistent with the conclusions of the previous sections: the impact of interactive aerosols prognostic effect is most pronounced at night.

Forecasts at 12 h show a much smaller improvement of TOTAL_ASSIM compared to REF_ASSIM, even though it is still significant. RMSE is reduced by around 5%, and a small negative bias is further decreased by TOTAL_ASSIM. The largest improvement in terms of RMSE occurs again at Siwa. For coastal stations, there is not much difference between TOTAL_ASSIM and REF_ASSIM. Forecasts at 24 h show a large negative bias for REF_ASSIM; this bias is more than corrected by TOTAL_ASSIM which shows a small positive bias. The improvement is very important at Cairo, while at Siwa the RMSE is much worse with TOTAL_ASSIM. The differences are not significant for 36 h forecasts.

It appears that the overall improvement brought by TOTAL_ASSIM is important for the initial conditions and short-term forecasts, and decreases with forecast times. Also,

Positive feedback of dust aerosol

S. Remy et al.

Title Page

Abstract

Introduction

Conclusions

References

Tables

Figures



Back

Close

Full Screen / Esc

Printer-friendly Version

Interactive Discussion



Positive feedback of dust aerosol

S. Remy et al.

[Title Page](#)[Abstract](#)[Introduction](#)[Conclusions](#)[References](#)[Tables](#)[Figures](#)[⏪](#)[⏩](#)[◀](#)[▶](#)[Back](#)[Close](#)[Full Screen / Esc](#)[Printer-friendly Version](#)[Interactive Discussion](#)

the impact and the improvements are more important during the night than during the day, as the cold bias of REF_ASSIM is mostly removed in TOTAL_ASSIM for the forecast times of 3 and 24 h. This is probably because the errors on the amount of dust and on the location/timing of the dust storm increase with forecast time. As a consequence, errors caused by the radiative impact of aerosols also grow with forecast time, which counterbalance the very positive impact that the prognostic aerosols radiative impact show on the analysis and short-term forecasts.

7.1.2 AOD forecasts

Figure 18 shows the RMSE and bias of AOD forecasted by REF_ASSIM and TOTAL_ASSIM against 32 African AERONET stations. The pre-operational MACC system is also displayed on this plot. It runs at a lower horizontal resolution: T_L255 horizontal spectral resolution, which corresponds to a grid-box size of about 80 km, instead of T_L511 , and uses a different model cycle than the REF_ASSIM and TOTAL_ASSIM experiments.

The positive feedback between dust AOD and boundary layer meteorology appears clearly, as TOTAL_ASSIM reduces the generally negative bias of REF_ASSIM. On average, for AOD, TOTAL_ASSIM brings a significant improvement in terms of bias, and a small one for RMSE. The same statistics were run over Europe, using 66 AERONET stations (not shown); there are no differences between REF_ASSIM and TOTAL_ASSIM except on 18 and 19 April 2012: as the dust storm impacted Turkey and Eastern Europe, the scores are improved significantly on these two days: RMSE is smaller by more than 10 % on 18 April 2012 for TOTAL_ASSIM.

8 Summary

The most significant interaction between aerosols and meteorology, as shown by these experiments was the following: increased down-welling long-wave radiation brought

Positive feedback of dust aerosol

S. Remy et al.

Title Page

Abstract

Introduction

Conclusions

References

Tables

Figures



Back

Close

Full Screen / Esc

Printer-friendly Version

Interactive Discussion



by the dust aerosol layer increased surface temperatures over land by up to 5–6 K at places. At higher altitude, the aerosol layer did not bring as much heating; as a consequence of higher surface temperatures, the thermal stratification of the lower atmosphere was less stable and more neutral. This in turn affected the wind profiles over the affected areas, which got closer to a linear profile that is typical of neutral boundary layers. This brought higher wind speeds at the surface (but not at 925 hPa), which in turned increased the production of dust aerosols through saltation processes.

The aerosol radiative effect on the long-wave spectrum also brought localized higher temperatures at 850 hPa. Associated with higher temperatures at surface, this deepened slightly the heat low over the desert at night. This in turn increased locally wind speeds and dust aerosol production. For the considered situation, this synoptic scale interaction was less significant than the one described above.

The aerosols radiative effect in the shortwave spectrum had an opposite interaction as the one described above: lower maximal temperatures increased the stability of the atmosphere, thus decreasing winds and aerosol production. However, this feedback was much smaller than the interaction of aerosols with the meteorology brought by the radiative impacts of aerosols in the long-wave spectrum. Assimilation runs confirmed this feedback, as it translated into the initial conditions of both aerosols and temperature. As the considered region does not have much observations of both temperature and total AOD from MODIS to constrain the initial conditions, the first guess has an unusually large importance in the initial conditions. Scores on surface temperatures and on AOD showed that the forecasts were of better quality when using prognostic aerosols instead of the Tegen aerosol climatology to compute the aerosols-radiation interaction, for forecast times up to 36 h.

Longer forecasts for another period, July 2012 (see Table 1), also showed that this feedback between atmospheric stability and interactive aerosols direct effect has a global impact in the MACC-II global system forecasts, outside of exceptional events like the dust storm of 17–18 April 2012.

9 Conclusions

We studied feedback effects between dust aerosols and radiation and associated changes in the meteorological parameters in the PBL with the MACC-II global system during the dust storm of 17–19 April 2012 in the Eastern Mediterranean. Simulations that use either the Tegen aerosol climatology or the prognostics aerosol forecast by the MACC model to compute the aerosol direct effect were compared. Dust aerosols were shown to have significant impact on downward radiative fluxes, reducing the short-wave component and increasing the long-wave one. That radiative impact affected in turn surface temperature, and thus lower atmosphere stability. This in turn led to an increase in wind speeds and an enhanced dust production. Overall, for this situation, the aerosol-radiation interaction on the long-wave spectrum had more impact on atmospheric stability and dust aerosol production than the aerosol-radiation interaction on the short-wave spectrum.

Compared against observations, downward radiative fluxes, both in the short-wave and in the long-wave spectrum, are better forecasted in this situation when using interactive aerosols to compute the aerosol-radiation interaction. Surface temperatures and dust AOD itself were better forecasted for short-term forecasts, as the aerosol plume is by then forecasted with a relatively small error. For larger forecast times, the fact that errors in the prediction of the location and timing of aerosol layers are larger can make the prognostic aerosol direct effect have a negative impact. There exist however alternatives between full prognostic aerosol direct effect and climatological aerosol direct effect. Prognostic aerosol direct effect can be used only in the short forecast that is used as the first guess in the assimilation step for example, thus bringing an improvement in the aerosol and temperatures analysis. Prognostic aerosol direct effect could also be relaxed towards climatological aerosol direct effect, depending on the forecast time.

Positive feedback of dust aerosol

S. Remy et al.

Title Page

Abstract

Introduction

Conclusions

References

Tables

Figures



Back

Close

Full Screen / Esc

Printer-friendly Version

Interactive Discussion



Acknowledgements. We thank NASA for providing the MODIS data, and the AERONET and BSRN projects for making their data freely and easily available. The authors also wish to thank Robin Hogan for his useful suggestions. This research was supported by the EU Seventh Research Framework Programme (MACC-II project, contract number 283576).

References

- Banta, R. M., Newsom, R. K., Lundquist, J. K., Pichugina, Y. L., Coulter, R. L., and Mahrt, L.: Nocturnal low-level jet characteristics over Kansas during CASES-99, *Bound.-Lay. Meteorol.*, 105, 221–252, 2002. 28169
- Bellouin, N., Boucher, O., Haywood, J., and Shekar Reddy, M.: Global estimate of aerosol direct radiative forcing from satellite measurements, *Nature*, 438, 1138–1141, 2005. 28149
- Benedetti, A., Morcrette, J.-J., Boucher, O., Dethof, A., Engelen, R. J., Fisher, M., Flentje, H., Huneeus, N., Jones, L., Kaiser, J. W., Kinne, S., Mangold, A., Razinger, M., Simmons, A. J., and Suttie, M.: Aerosol analysis and forecast in the European Centre for Medium-Range Weather Forecasts Integrated Forecast System: 2. Data assimilation, *J. Geophys. Res.*, 114, D13205, doi:10.1029/2008JD011115, 2009. 28152
- Boucher, O., Pham, M., and Venkataraman, C.: Simulation of the Atmospheric Sulfur Cycle in the LMD GCM: Model Description, Model Evaluation, and Global and European Budgets, *Inst. Pierre-Simon Laplace, Paris, France*, note 23, 26 pp., 2002. 28151
- Choi, J.-O. and Chung, C.-E.: Sensitivity of aerosol direct radiative forcing to aerosol vertical profile, *Tellus B*, 66, 24376, doi:10.3402/tellusb.v66.24376, 2014. 28149
- Ginoux, P., Chin, M., Tegen, I., Prospero, J., Holben, B. N., Dubovik, O., and Lin, S.-J.: Sources and distributions of dust aerosols simulated with the GOCART model, *J. Geophys. Res.*, 106, 20255–20274, 2001. 28152
- Haywood, J. M., Osborne, S. R., Francis, P. N., Kiel, A., Formenti, P., Andreae, M. O., and Kaye, P. H.: The mean physical and optical properties of regional haze dominated by biomass burning aerosol measured from the C-130 aircraft during SAFARI 2000, *J. Geophys. Res.*, 108, 8473, doi:10.1029/2002JD002226, 2003. 28151
- Heimo, A., Vernez, A., and Wasserfallen, P.: Baseline Surface Radiation Network (BSRN). Concept and Implementation of a BSRN Station, WMO/td-no. 579, World Meteorological Organization, Geneva, Switzerland, 1993. 28153

**Positive feedback of
dust aerosol**

S. Remy et al.

Title Page

Abstract

Introduction

Conclusions

References

Tables

Figures



Back

Close

Full Screen / Esc

Printer-friendly Version

Interactive Discussion



- Heinhold, A., Tegen, I., Schepanski, I., and Hellmuth, O.: Dust radiative feedback on Saharan boundary layer dynamics and dust mobilization, *Geophys. Res. Lett.*, 35, L20817, doi:10.1029/2008GL035319, 2008. 28150
- Holben, B. N., Eck, T. F., Slutsker, I., Tanré, D., Buis, J. P., Setzer, A., Vermote, E., Reagan, J. A., Kaufman, Y., Nakajima, T., Lavenu, F., Jankowiak, I., and Smirnov, A.: AERONET – a federated instrument network and data archive for aerosol characterization, *Remote Sens. Environ.*, 66, 1–16, 1998. 28153
- Hollingsworth, A., Engelen, R. J., Textor, C., Benedetti, A., Boucher, O., Chevallier, F., Dehtof, A., Elbern, H., Eskes, H., Flemming, J., Granier, C., Kaiser, J. W., Morcrette, J.-J., Rayner, P., Peuch, V.-H., Rouil, L., Schultz, M. G., and Simmons, A. J.: Toward a monitoring and forecasting system for atmospheric composition: the GEMS project, *B. Am. Meteorol. Soc.*, 89, 1147–1164, 2008. 28151
- Inness, A., Baier, F., Benedetti, A., Bouarar, I., Chabrilat, S., Clark, H., Clerbaux, C., Coheur, P., Engelen, R. J., Errera, Q., Flemming, J., George, M., Granier, C., Hadji-Lazaro, J., Huijnen, V., Hurtmans, D., Jones, L., Kaiser, J. W., Kapsomenakis, J., Lefever, K., Leitão, J., Razingier, M., Richter, A., Schultz, M. G., Simmons, A. J., Suttie, M., Stein, O., Thépaut, J.-N., Thouret, V., Vrekoussis, M., Zerefos, C., and the MACC team: The MACC reanalysis: an 8 yr data set of atmospheric composition, *Atmos. Chem. Phys.*, 13, 4073–4109, doi:10.5194/acp-13-4073-2013, 2013.
- Boucher, O., Randall, D., Artaxo, P., Bretherton, C., Feingold, G., Forster, P., Kerminen, V.-M., Kondo, Y., Liao, H., Lohmann, U., Rasch, P., Satheesh, S. K., Sherwood, S., Stevens, B., and Zhang, X. Y.: Clouds and aerosols, in: *Climate Change: The Physical Science Basis. Contribution of Working Group I to the Fifth Assessment Report*, edited by: Stocker, T. F., Qin, D., Plattner, G.-K., Tignor, M., Allen, S. K., Boschung, J., Nauels, A., Xia, Y., Bex, V., and Midgley, P. M., Cambridge University Press, Cambridge, UK and New York, NY, USA, 2013. 28149, 28150
- Kamal, M. M., Qu, J. J., and Hao, X.: A study of dust aerosols impact on hurricanes with multi-sensors measurement from space, *Open Remote Sens. J.*, 5, 73–82, 2012. 28150
- Koch, D. and Del Genio, A. D.: Black carbon semi-direct effects on cloud cover: review and synthesis, *Atmos. Chem. Phys.*, 10, 7685–7696, doi:10.5194/acp-10-7685-2010, 2010. 28149
- Lyubansky, V.: Meteorological synoptical observations from station Sede Boqer (2012-01), The Jacob Blaustein Institutes for Desert Research, Sede Boqer, doi:10.1594/PANGAEA.802681, 2012. 28153

Positive feedback of dust aerosol

S. Remy et al.

Title Page

Abstract

Introduction

Conclusions

References

Tables

Figures



Back

Close

Full Screen / Esc

Printer-friendly Version

Interactive Discussion



- Mimouni, M.: Basic measurements of radiation at station Tamanrasset (2013-09), National Meteorological Office of Algeria, doi:10.1594/PANGAEA.822372, 2013. 28153
- Mulcahy, J. P., Walters, D. N., Bellouin, N., and Milton, S. F.: Impacts of increasing the aerosol complexity in the Met Office global numerical weather prediction model, *Atmos. Chem. Phys.*, 14, 4749–4778, doi:10.5194/acp-14-4749-2014, 2014. 28150
- Morcrette, J.-J., Boucher, O., Jones, L., Salmond, D., Bechtold, B., Beljaars, A., Benedetti, A., Bonet, A., Kaiser, J. W., Razinger, M., Schulz, M., Serrar, S., Simmons, A. J., Sofiev, M., Suttie, M., Tompkins, A. M., and Untch, A.: Aerosol analysis and forecast in the European Centre for Medium-Range Weather Forecasts Integrated Forecast System: forward modeling, *J. Geophys. Res.*, 114, D06206, doi:10.1029/2008JD011235, 2009. 28151
- Painemal, D. and Zuidema, P.: The first aerosol indirect effect quantified through airborne remote sensing during VOCALS-REx, *Atmos. Chem. Phys.*, 13, 917–931, doi:10.5194/acp-13-917-2013, 2013. 28149
- Peuch, V.-H. and Engelen, R. J.: Towards and operational GMES Atmosphere Monitoring Service, *ECMWF Newsletter*, 132, 20–25, 2012. 28151
- Reale, O., Lau, K. M., and da Silva, A.: Impact of interactive aerosol on the African Easterly Jet in the NASA GEOS-5 Global Forecasting System, *Weather Forecast.*, 26, 504–519, 2011. 28150
- Reddy, M. S., Boucher, O., Bellouin, N., Schulz, M., Balkanski, Y., Dufresne, J.-L., and Pham, M.: Estimates of global multicomponent aerosol optical depth and direct radiative perturbation in the Laboratoire de Meteorologie Dynamique general circulation model, *J. Geophys. Res.*, 110, D10S16, doi:10.1029/2004JD004757, 2005. 28151
- Rodwell, M. J. and Jung, T.: Understanding the local and global impacts of model physics changes: an aerosol example, *Q. J. Roy. Meteor. Soc.*, 134, 1479–1497, 2008. 28150
- Schulz, M., Textor, C., Kinne, S., Balkanski, Y., Bauer, S., Berntsen, T., Berglen, T., Boucher, O., Dentener, F., Guibert, S., Isaksen, I. S. A., Iversen, T., Koch, D., Kirkevåg, A., Liu, X., Montanaro, V., Myhre, G., Penner, J. E., Pitari, G., Reddy, S., Seland, Ø., Stier, P., and Takemura, T.: Radiative forcing by aerosols as derived from the AeroCom present-day and pre-industrial simulations, *Atmos. Chem. Phys.*, 6, 5225–5246, doi:10.5194/acp-6-5225-2006, 2006. 28150
- Shi, Y., Zhang, J., Reid, J. S., Hyer, E. J., and Hsu, N. C.: Critical evaluation of the MODIS Deep Blue aerosol optical depth product for data assimilation over North Africa, *Atmos. Meas. Tech.*, 6, 949–969, doi:10.5194/amt-6-949-2013, 2013. 28154

Positive feedback of dust aerosol

S. Remy et al.

Title Page

Abstract

Introduction

Conclusions

References

Tables

Figures



Back

Close

Full Screen / Esc

Printer-friendly Version

Interactive Discussion



Stengel, M., Kniffka, A., Meirink, J. F., Riihelä, A., Trentmann, J., Müller, R., Lockhoff, M., and Hollmann, R.: CLAAS: CM SAF CCloud property dAtAset using SE-VIRI – edition 1 – hourly/daily means, pentad means, monthly means/monthly mean diurnal cycle/monthly histograms, Satellite Application Facility on Climate Monitoring
doi:10.5676/EUM_SAF_CM/CLAAS/V001, 2013. 28153

Stier, P., Schutgens, N. A. J., Bellouin, N., Bian, H., Boucher, O., Chin, M., Ghan, S., Huneus, N., Kinne, S., Lin, G., Ma, X., Myhre, G., Penner, J. E., Randles, C. A., Samset, B., Schulz, M., Takemura, T., Yu, F., Yu, H., and Zhou, C.: Host model uncertainties in aerosol radiative forcing estimates: results from the AeroCom Prescribed intercomparison study, *Atmos. Chem. Phys.*, 13, 3245–3270, doi:10.5194/acp-13-3245-2013, 2013. 28150

Sun, Y. L., Wang, Z. F., Fu, P. Q., Yang, T., Jiang, Q., Dong, H. B., Li, J., and Jia, J. J.: Aerosol composition, sources and processes during wintertime in Beijing, China, *Atmos. Chem. Phys.*, 13, 4577–4592, doi:10.5194/acp-13-4577-2013, 2013. 28149

Tegen, I., Hoorig, P., Chin, M., Fung, I., Jacob, D., and Penner, J.: Contribution of different aerosol species to the global aerosol extinction optical thickness: estimates from model results, *J. Geophys. Res.*, 102, 23895–23915, 1997. 28152, 28158, 28159

Tompkins, A. M., Cardinali, C., Morcrette, J. J., and Rodwell, M.: Influence of aerosol climatology on forecasts of the African Easterly Jet, *Geophys. Res. Lett.*, 32, L10801, doi:10.1029/2004GL022189, 2005. 28150

Yu, H., Kaufman, Y. J., Chin, M., Feingold, G., Remer, L. A., Anderson, T. L., Balkanski, Y., Bellouin, N., Boucher, O., Christopher, S., DeCola, P., Kahn, R., Koch, D., Loeb, N., Reddy, M. S., Schulz, M., Takemura, T., and Zhou, M.: A review of measurement-based assessments of the aerosol direct radiative effect and forcing, *Atmos. Chem. Phys.*, 6, 613–666, doi:10.5194/acp-6-613-2006, 2006. 28149

Zhang, J. K., Sun, Y., Liu, Z. R., Ji, D. S., Hu, B., Liu, Q., and Wang, Y. S.: Characterization of submicron aerosols during a month of serious pollution in Beijing, 2013, *Atmos. Chem. Phys.*, 14, 2887–2903, doi:10.5194/acp-14-2887-2014, 2014. 28149

**Positive feedback of
dust aerosol**

S. Remy et al.

[Title Page](#)[Abstract](#)[Introduction](#)[Conclusions](#)[References](#)[Tables](#)[Figures](#)[Back](#)[Close](#)[Full Screen / Esc](#)[Printer-friendly Version](#)[Interactive Discussion](#)

Table 1. Mean global dust AOD for July 2012 as a function of forecast time, REF, SW, LW and TOTAL experiments.

Forecast time	24 h	96 h	168 h	240 h
REF	0.0358	0.0355	0.0357	0.0358
SW	0.0358	0.0348	0.0340	0.0330
LW	0.0374	0.0381	0.0391	0.0393
TOTAL	0.0373	0.0380	0.0390	0.0393

Positive feedback of dust aerosol

S. Remy et al.

Title Page

Abstract

Introduction

Conclusions

References

Tables

Figures



Back

Close

Full Screen / Esc

Printer-friendly Version

Interactive Discussion



Table 2. 2 m temperature, RMSE of REF_ASSIM (left) and TOTAL_ASSIM (right) for forecast times 3, 12, 24 and 36 h, average for the period of 10 to 25 April 2012. Stations considered are Hurguada, Dabaa, Luxor, Kosseir, Siwa, Wadi el Natroon, Cairo, Port Said and Ras Sedr in Egypt, and Ben Gurion airport close to Tel Aviv in Israel.

Forecast time	3 h	12 h	24 h	36 h
REF_ASSIM	2.02	1.68	1.91	1.69
TOTAL_ASSIM	1.75	1.62	1.83	1.67

Positive feedback of dust aerosol

S. Remy et al.

Title Page

Abstract

Introduction

Conclusions

References

Tables

Figures



Back

Close

Full Screen / Esc

Printer-friendly Version

Interactive Discussion



Table 3. 2 m temperature, bias of REF_ASSIM (left) and TOTAL_ASSIM (right) for forecast times 3, 12, 24 and 36 h, average for the period of 10 to 25 April 2012 over the same selection of weather stations as Table 2.

Forecast time	3 h	12 h	24 h	36 h
REF_ASSIM	-1.21	-0.32	-0.99	0.11
TOTAL_ASSIM	-0.16	-0.18	-0.37	0.23

Positive feedback of
dust aerosol

S. Remy et al.

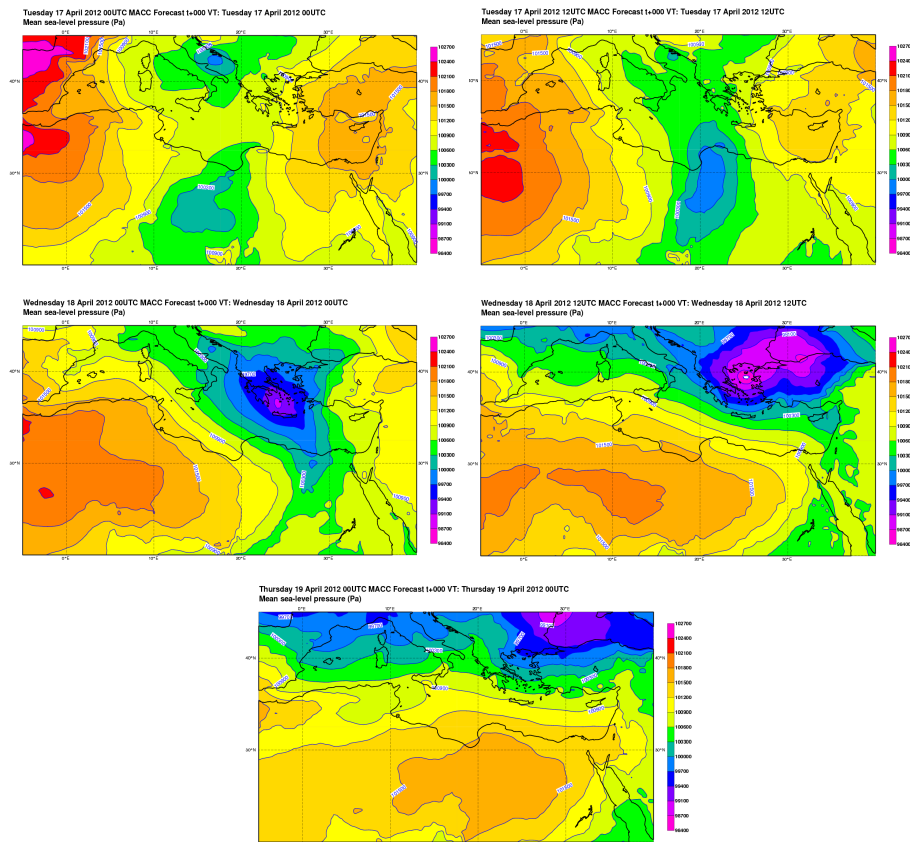


Figure 1. Analysis of mean sea-level pressure over Northern Sahara and Southern Mediterranean from 17 April 2012 00:00 UTC to 19 April 2012 00:00 UTC.

Positive feedback of
dust aerosol

S. Remy et al.

Title Page

Abstract

Introduction

Conclusions

References

Tables

Figures

◀

▶

◀

▶

Back

Close

Full Screen / Esc

Printer-friendly Version

Interactive Discussion

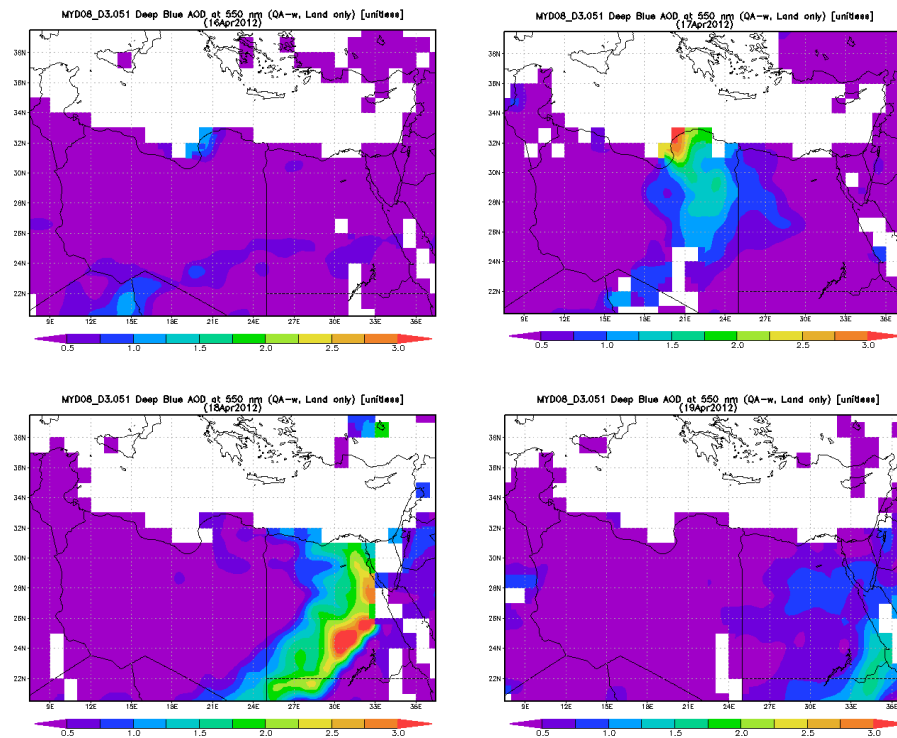


Figure 2. AOD at 550 nm from MODIS on Aqua, deep blue algorithm, daily average for 16, 17, 18 and 19 April 2012.

Positive feedback of dust aerosol

S. Remy et al.

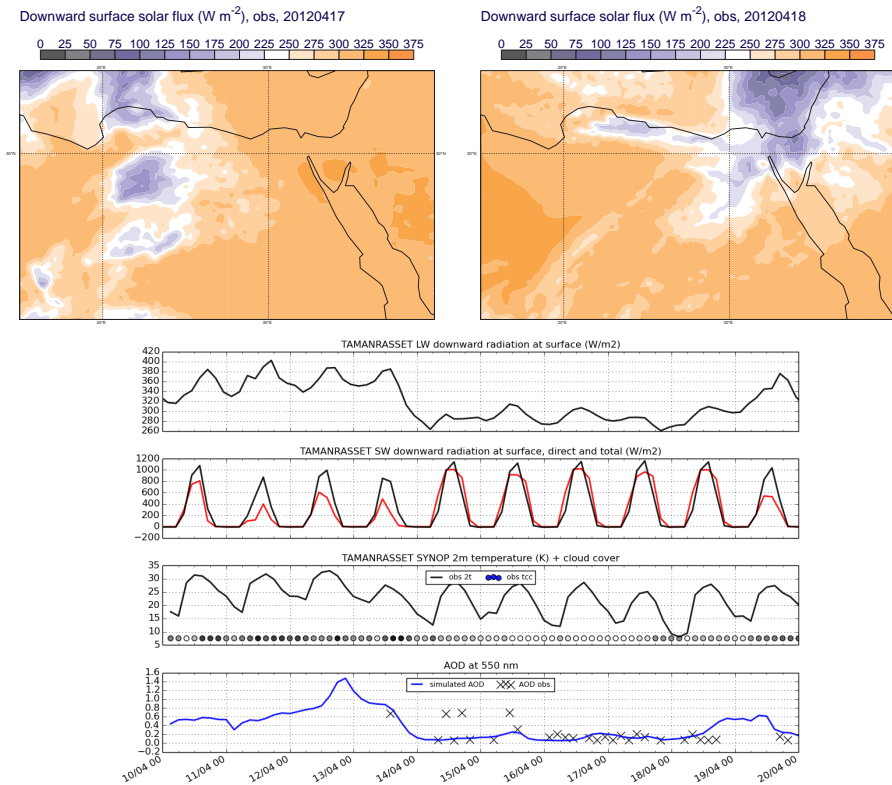


Figure 3. Daily average of surface incoming shortwave radiation from CM-SAF, on 17 and 18 April 2012, in $W m^{-2}$. On the bottom is a visible image from MODIS/Aqua on 18 April 2012 at 13:00 UTC.

Title Page

Abstract Introduction

Conclusions References

Tables Figures

◀ ▶

◀ ▶

Back Close

Full Screen / Esc

Printer-friendly Version

Interactive Discussion



Positive feedback of dust aerosol

S. Remy et al.

Title Page

Abstract

Introduction

Conclusions

References

Tables

Figures



Back

Close

Full Screen / Esc

Printer-friendly Version

Interactive Discussion

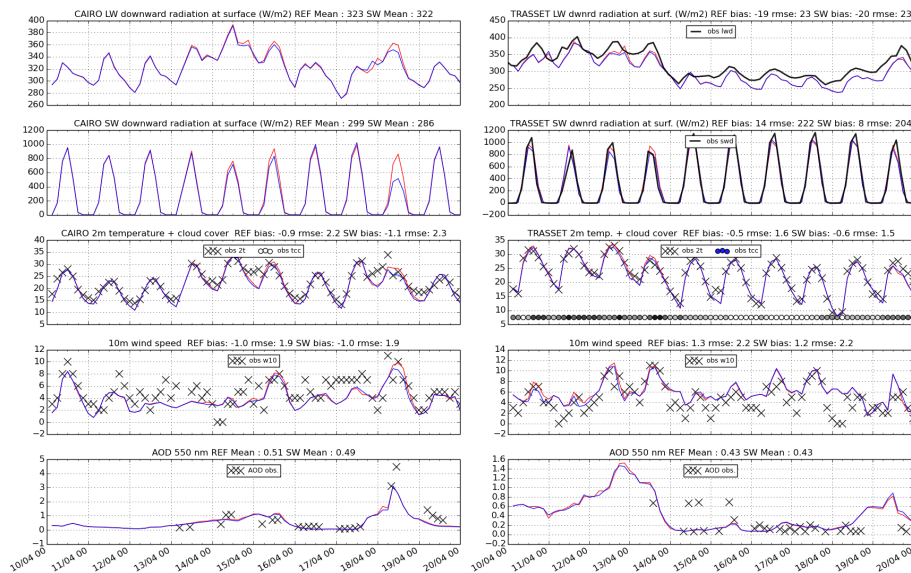


Figure 4. 3 to 24 h forecasts and observations (when available) of downward shortwave and long-wave radiation fluxes at the surface, of 2 m temperature, total cloud cover, 10 m wind speed, mean sea-level pressure and AOD at 550 nm at Cairo and Tamarasset. REF experiment is in red, SW is in blue, observations in black (when available). The bias and RMSE of forecasts against observations for the whole period is also indicated on top.

Positive feedback of dust aerosol

S. Remy et al.

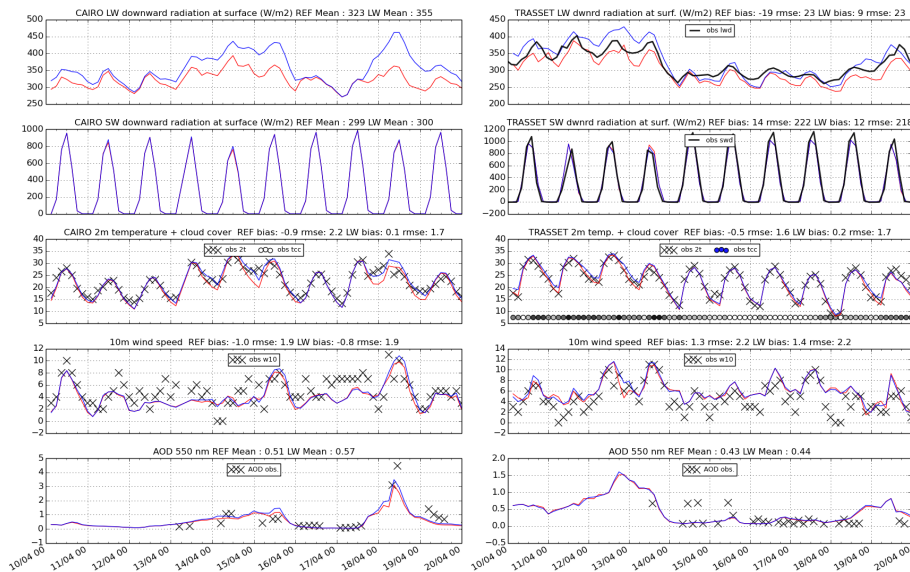


Figure 5. 3 to 24 h forecasts and observations (when available) of downward shortwave and long-wave radiation fluxes at the surface, of 2 m temperature, total cloud cover, 10 m wind speed, mean sea-level pressure and AOD at 550 nm at Cairo and Tamarasset. REF experiment is in red, LW is in blue, observations in black (when available). The bias and RMSE of forecasts against observations for the whole period is also indicated on top.

Title Page

Abstract

Introduction

Conclusions

References

Tables

Figures



Back

Close

Full Screen / Esc

Printer-friendly Version

Interactive Discussion



Positive feedback of dust aerosol

S. Remy et al.

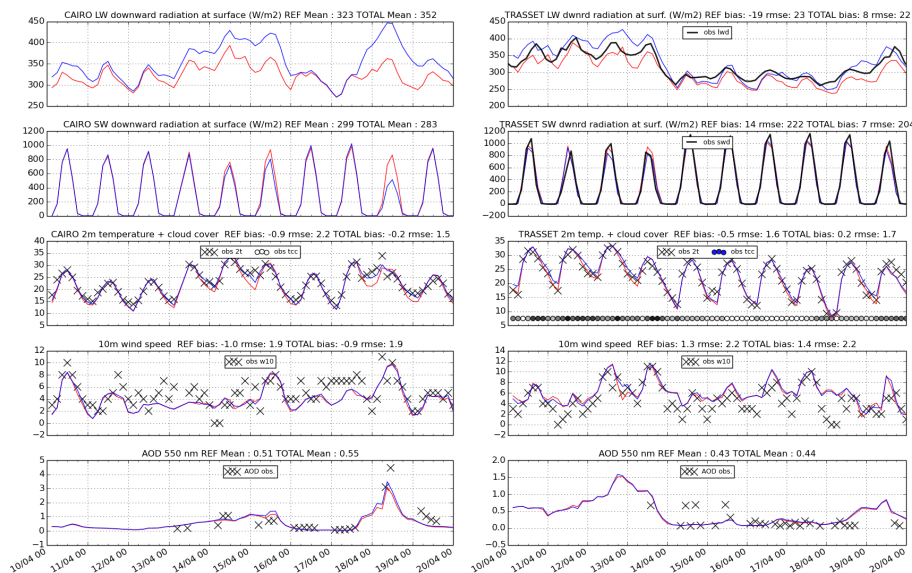


Figure 6. 3 to 24 h forecasts and observations (when available) of downward shortwave and long-wave radiation fluxes at the surface, of 2 m temperature, total cloud cover, 10 m wind speed, mean sea-level pressure and AOD at 550 nm at Cairo and Tamarasset. REF experiment is in red, TOTAL is in blue, observations in black (when available). The bias and RMSE of forecasts against observations for the whole period is also indicated on top.

Positive feedback of dust aerosol

S. Remy et al.

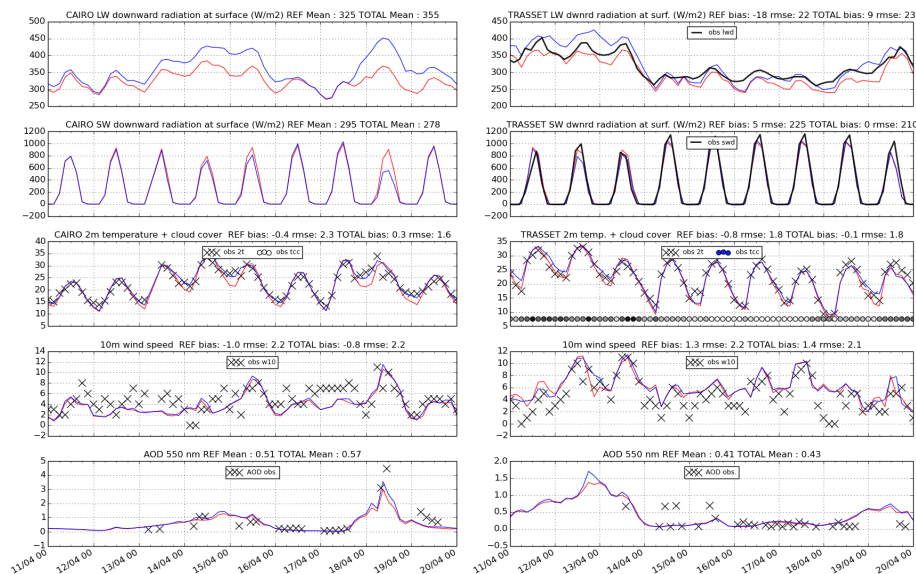


Figure 7. 24 to 45 h forecasts and observations (when available) of downward shortwave and long-wave radiation fluxes at the surface, of 2 m temperature, total cloud cover, 10 m wind speed, mean sea-level pressure and AOD at 550 nm at Cairo and Tamarasset. REF experiment is in red, TOTAL is in blue, observations in black (when available). The bias and RMSE of forecasts against observations for the whole period is also indicated on top.

Title Page

Abstract

Introduction

Conclusions

References

Tables

Figures



Back

Close

Full Screen / Esc

Printer-friendly Version

Interactive Discussion



Positive feedback of
dust aerosol

S. Remy et al.

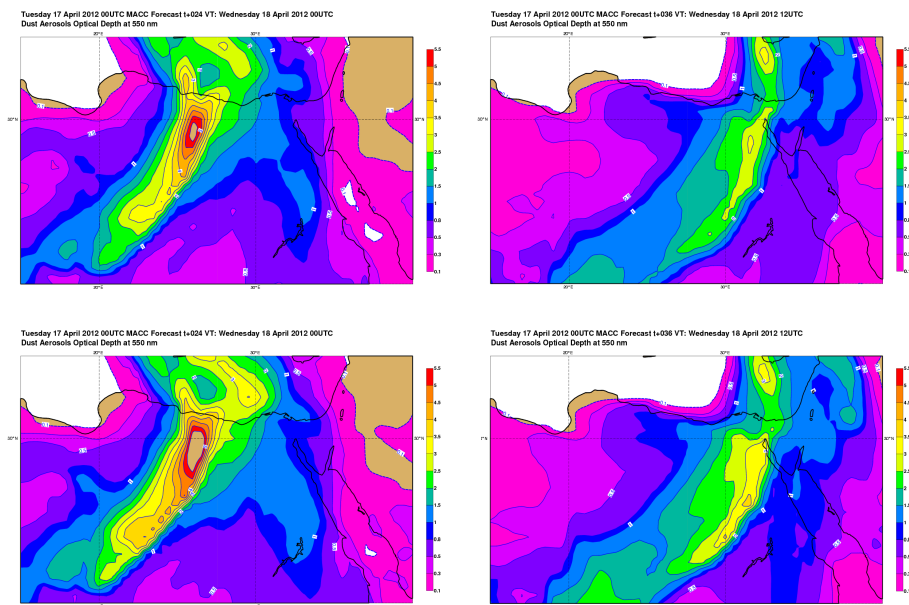


Figure 8. AOD at 550 nm, simulations starting on 17 April 2012 00:00 UTC, 24 h forecast (left) and 36 h forecast (right). REF experiment on the top, TOTAL on the bottom.

Positive feedback of dust aerosol

S. Remy et al.

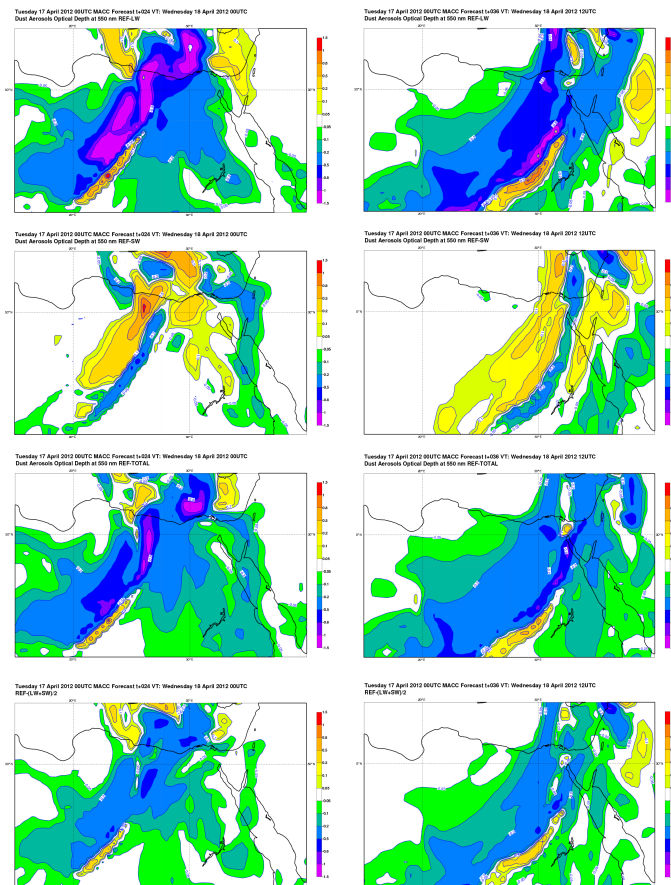


Figure 9. Simulations starting on 17 April 2012, 24 h forecast (left) and 36 h forecast (right). Dust AOD, REF minus LW (top), REF minus SW (middle top), REF – TOTAL (middle bottom), TOTAL minus the average of SW and LW, bottom.

Positive feedback of
dust aerosol

S. Remy et al.

Title Page

Abstract

Introduction

Conclusions

References

Tables

Figures



Back

Close

Full Screen / Esc

Printer-friendly Version

Interactive Discussion

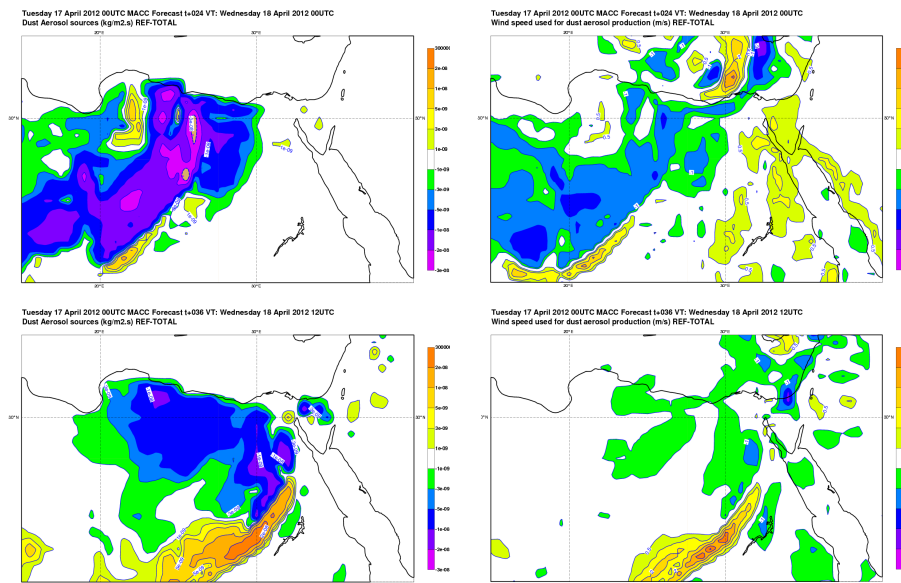


Figure 10. Difference REF – TOTAL for dust aerosol production flux (left) and wind speed at 10 m (right), simulations starting on 17 April 2012, 24 h forecast (top) and 36 h forecast (bottom).

Positive feedback of dust aerosol

S. Remy et al.

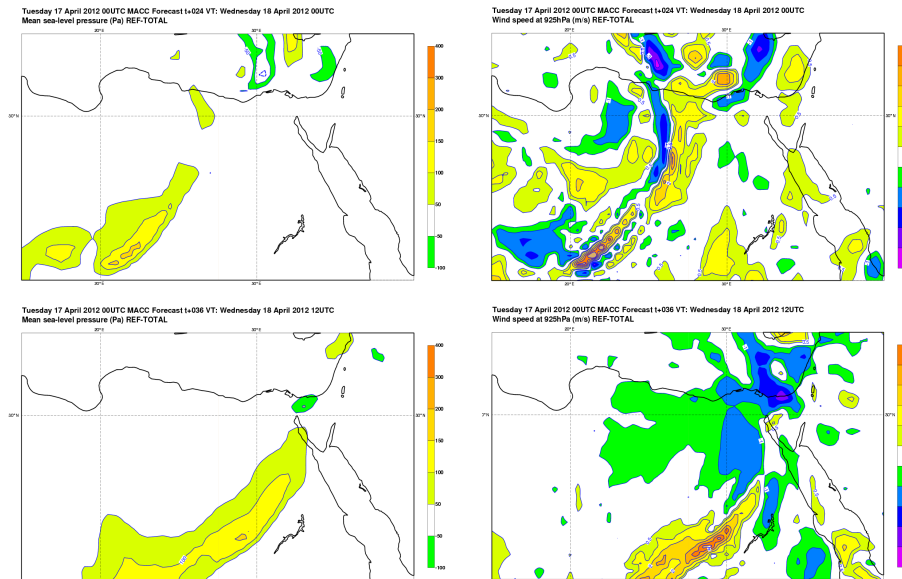


Figure 11. Difference REF – TOTAL for sea-level pressure (left) and wind speed at 925 hPa (right), simulations starting on 17 April 2012, 24 h forecast (top) and 36 h forecast (bottom).

Title Page

Abstract

Introduction

Conclusions

References

Tables

Figures



Back

Close

Full Screen / Esc

Printer-friendly Version

Interactive Discussion



Positive feedback of dust aerosol

S. Remy et al.

Title Page

Abstract

Introduction

Conclusions

References

Tables

Figures

◀

▶

◀

▶

Back

Close

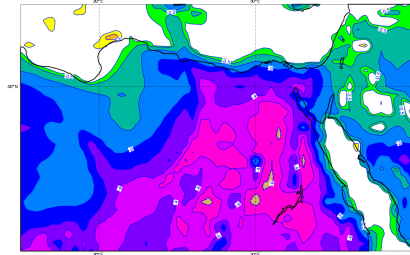
Full Screen / Esc

Printer-friendly Version

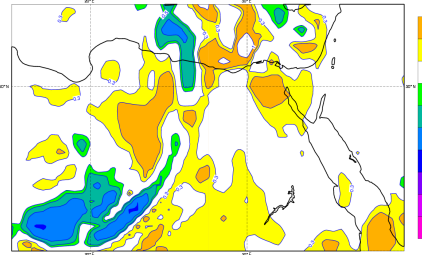
Interactive Discussion



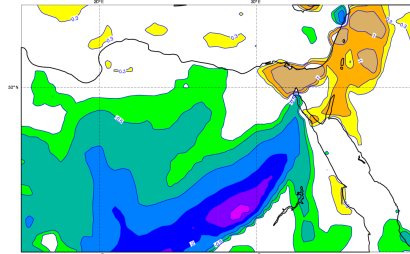
Tuesday 17 April 2012 00UTC MACC Forecast 1+024 VT; Wednesday 18 April 2012 00UTC
2m temperature (K) REF-TOTAL



Tuesday 17 April 2012 00UTC MACC Forecast 1+024 VT; Wednesday 18 April 2012 00UTC
850 hPa temperature (K) REF-TOTAL



Tuesday 17 April 2012 00UTC MACC Forecast 1+036 VT; Wednesday 18 April 2012 12UTC
2m temperature (K) REF-TOTAL



Tuesday 17 April 2012 00UTC MACC Forecast 1+036 VT; Wednesday 18 April 2012 12UTC
850 hPa temperature (K) REF-TOTAL

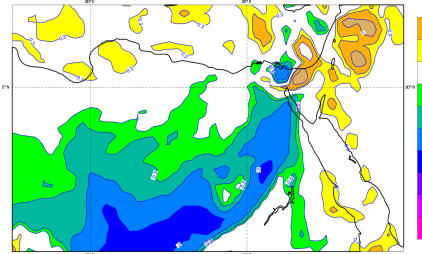


Figure 12. Difference REF – TOTAL for 2 m temperature (left) and 850 hPa temperature (right), simulations starting on 17 April 2012, 24 h forecast (top) and 36 h forecast (bottom).

Positive feedback of dust aerosol

S. Remy et al.

Title Page

Abstract

Introduction

Conclusions

References

Tables

Figures



Back

Close

Full Screen / Esc

Printer-friendly Version

Interactive Discussion

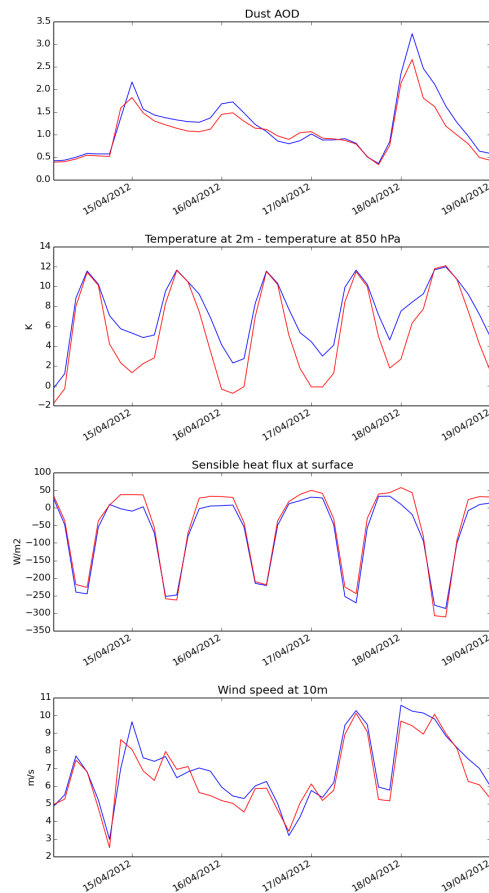


Figure 13. Time evolution of REF (red) and TOTAL (blue), 3–24 h forecasts starting at 00:00 UTC every day, at 22.5° N, 22° E. AOD (top), 2 m temperature – 850 hPa temperature (middle top), surface heat flux (middle bottom) and 10 m wind speed (bottom).

Positive feedback of dust aerosol

S. Remy et al.

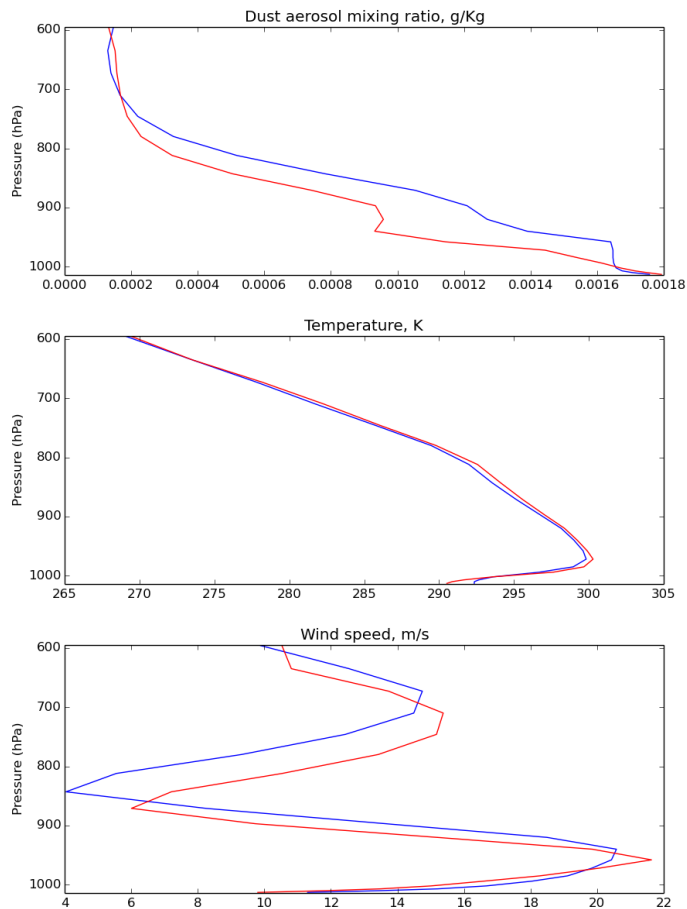


Figure 14. Vertical profile of dust aerosol mixing ratio (top), temperature (middle) and wind speed (bottom) at 22.5° N, 22° E, 24 h forecast starting on 17 April 2012. REF is in red, TOTAL in blue.

Positive feedback of dust aerosol

S. Remy et al.

Title Page

Abstract

Introduction

Conclusions

References

Tables

Figures



Back

Close

Full Screen / Esc

Printer-friendly Version

Interactive Discussion

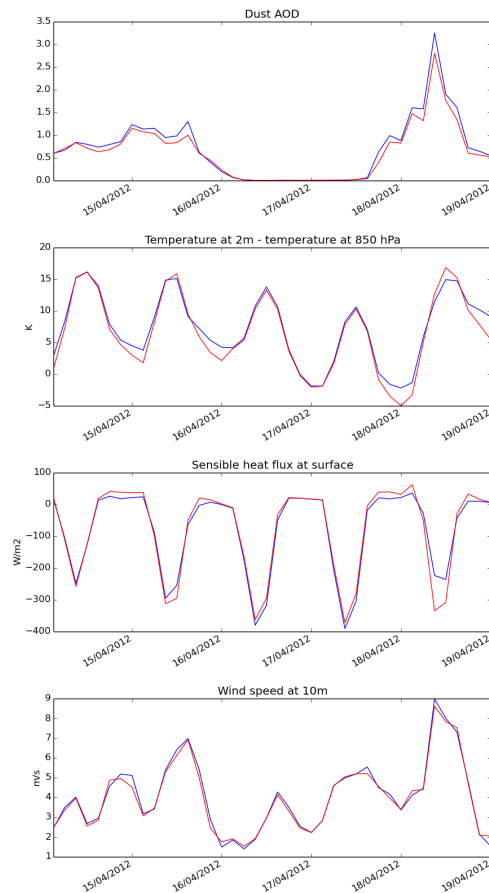


Figure 15. Time evolution of REF (red) and TOTAL (blue), 3–24 h forecasts starting at 00:00 UTC every day, at 31° N, 32° E. AOD (top), 2 m temperature – 850 hPa temperature (mid-top), surface heat flux (middle bottom) and 10 m wind speed (bottom).

Positive feedback of dust aerosol

S. Remy et al.

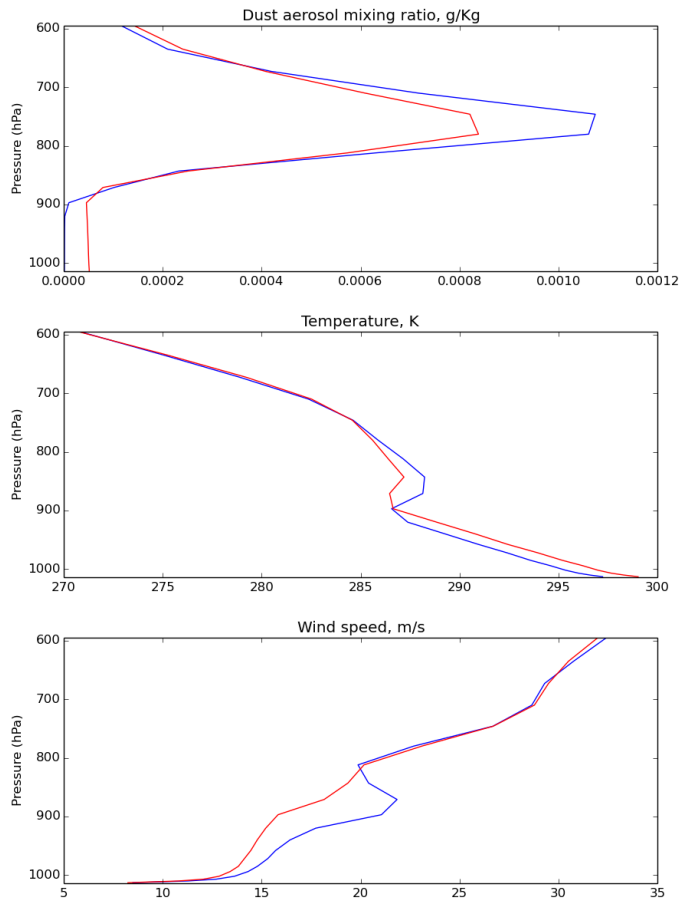


Figure 16. Vertical profile of dust aerosol mixing ratio (top), temperature (middle) and wind speed (bottom) at 31° N, 32° E, 36 h forecast starting on 17 April 2012. REF is in red, TOTAL in blue.

[Title Page](#)[Abstract](#)[Introduction](#)[Conclusions](#)[References](#)[Tables](#)[Figures](#)[◀](#)[▶](#)[◀](#)[▶](#)[Back](#)[Close](#)[Full Screen / Esc](#)[Printer-friendly Version](#)[Interactive Discussion](#)

Positive feedback of dust aerosol

S. Remy et al.

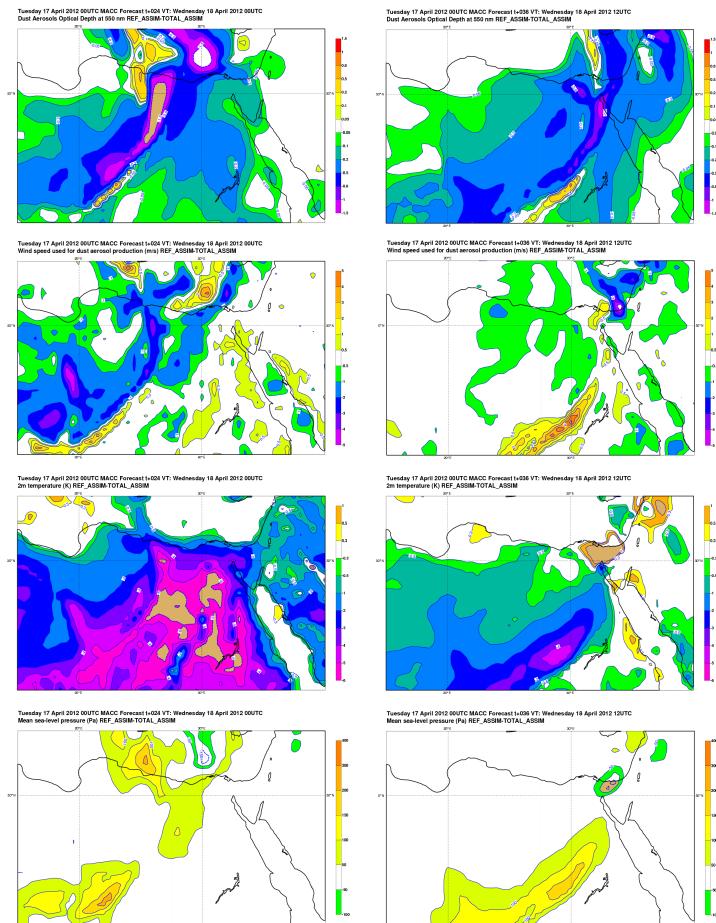


Figure 17. Simulations SOUTC starting on 17 April 2012, 24 h forecast (left) and 36 h forecast (right). Difference REF_ASSIM – TOTAL_ASSIM for dust aerosol AOD (top), 10 m wind speed (middle top), 2 m temperature (middle bottom) and mean sea-level pressure (bottom).

Positive feedback of dust aerosol

S. Remy et al.

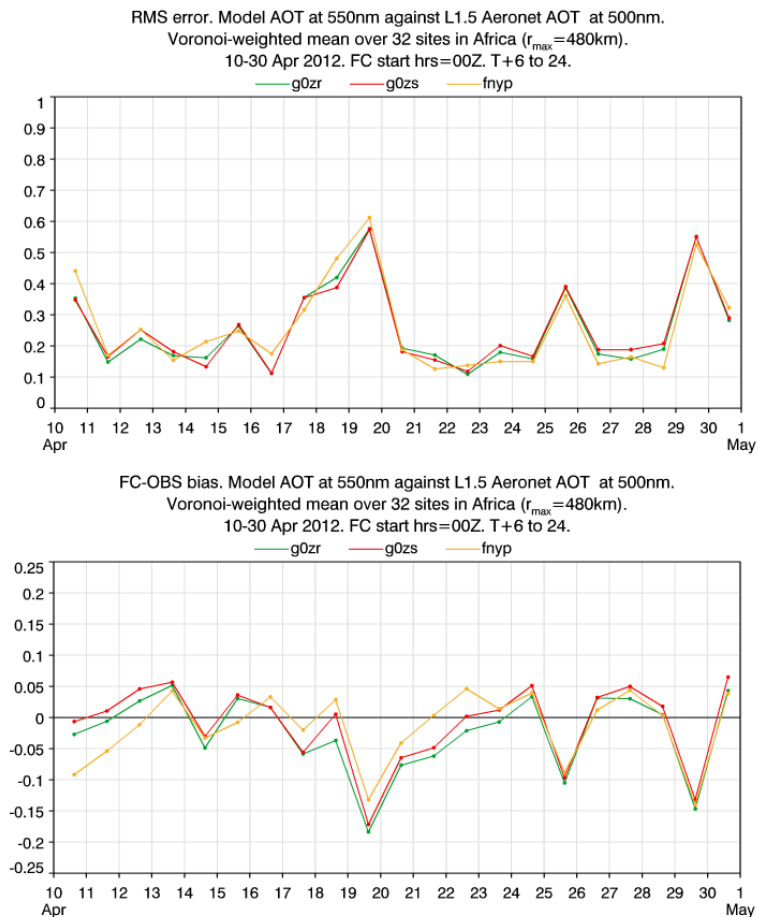


Figure 18. RMSE (top) and bias (bottom) against L1.5 Aeronet AOT at 500 nm. Voronoi-weighted mean over 32 sites in Africa, forecast times 6 to 24 h, 10–30 April 2012. Green is REF_ASSIM, red is TOTAL_ASSIM and yellow is the pre-operational global MACC system.

